Physics – Uspekhi **68** (9) 857 – 882 (2025)

REVIEWS OF TOPICAL PROBLEMS

PACS numbers: 03.65.Ud, **03.67. – a**, 42.50.Ex

INTERNATIONAL YEAR OF QUANTUM SCIENCE AND TECHNOLOGY

Quantum repeaters: current research trends and latest achievements

R.A. Akhmedzhanov, Yu.Yu. Balega, A.D. Deev, A.A. Kalachev

DOI: https://doi.org/10.3367/UFNe.2025.05.039918

Contents

Abstract. We present a review of current theoretical and experimental studies focused on the development of a quantum repeater, a key device for extended quantum networks that allows entangled states to be distributed over long distances. We also consider the most promising approaches to designing basic devices for quantum repeaters, including quantum memory, sources of nonclassical states of light, and quantum frequency converters.

Keywords: quantum repeaters, optical quantum memory, single-photon sources, two-photon sources, entanglement, quantum frequency converters

R.A. Akhmedzhanov [1, a], **Yu.Yu. Balega** [2, b], **A.D. Deev** [3, 4, c], **A.A. Kalachev** [5, d]
[1] Federal Research Center A.V. Gaponov-Grekhov Institute of Applied Physics, Russian Academy of Sciences, ul. Ul'yanova 46, 603000 Nizhny Novgorod, Russian Federation
[2] Russian Academy of Sciences, China Branch of BRICS Institute of Future Networks, Shenzhen, China
[3] Moscow Institute of Physics and Technology (National Research University), Institutskii per. 9, 141701 Dolgoprudnyi, Moscow region, Russian Federation
[4] R&D Center JSC, Bol'shoi Balkanskii per. 20, 129090 Moscow, Russian Federation
[5] Federal Research Center Kazan Scientific Center, Russian Academy of Sciences, ul. Lobachevskogo 2/31, 420111 Kazan, Russian Federation
E-mail: [a] rinat@ipfran.ru, [b] balega@sao.ru, [c] andreydeevmsu@gmail.com, [d] a.a.kalachev@mail.ru

Received 24 April 2024, revised 18 May 2025
Uspekhi Fizicheskikh Nauk **195** (9) 909 – 938 (2025)
Translated by I.A. Ulitkin

1. Introduction

The development of quantum networks that allow quantum information to be transmitted over long distances is one of the most relevant issues in the field of quantum technologies. Its solution can significantly expand the frontiers of quantum communication, quantum computing, and quantum metrology. In particular, quantum networks are necessary for long-range quantum key distribution with untrusted nodes [1, 2], unification of quantum processors for distributed quantum computing [3–9], blind quantum computing [10–13], quantum clock synchronization [14–20], distributed quantum measurements [21–32], increasing the accuracy of astronomical observations [33–35], and other applications (see reviews [36–39]). In general, the point at issue is the development of the quantum Internet, the use of which—together with the conventional Internet — will markedly expand the capabilities of information distribution and processing. Presently, there are only demonstrations of the simplest quantum networks that allow three quantum nodes to be entangled within a laboratory (see review [40]), and the first experiments on distributing entanglement between nodes separated by a distance of about 10 km have been conducted [41–43]. The development of fully functional quantum networks capable of transmitting and controlling entangled quantum states in field conditions is an important research topic in the field of quantum technology and requires sustained and coordinated efforts in the fields of physics, computer science, and engineering. Nevertheless, quantum network architectures, where problems of routing, resource allocation, etc., are solved, are already being actively discussed [44–46]. In addition, much attention is directed to simulating quantum networks and developing the corresponding software (see reviews [39, 47]).

The key point in the functioning of quantum networks is the distribution of entangled quantum states between remote nodes. However, losses in typical quantum channels, such as fiber or atmospheric optical communication lines, make it almost impossible to directly transmit quantum states over long distances. For example, in an optical fiber with a loss of 0.2 dB km^{-1}, 99% of photons are lost every 100 km, so that, when transmitting 10^{10} photons per second through a 1000-km-long fiber, the rate of their reception will be about 1 photon every 175 years. As a result, the range of quantum communication is limited to a distance of about 100 km (see, for example, experiments on quantum teleportation [48, 49]). It is important to note that, unlike classical optical communication systems, amplification of optical signals in intermediate nodes (repeaters) is impossible in quantum networks, which is explained by the impossibility of cloning unknown quantum states [50]. The only currently available solution is the use of trusted intermediate nodes [51], which convert quantum information into classical information. This approach enables long-range quantum key distribution (see, for example, [52]); however, it is not suitable for distributing quantum states and constructing quantum networks.

A promising approach to building large-scale quantum networks is the use of quantum repeaters [53, 54], i.e., intermediate nodes in which quantum information can be stored for some time in memory devices in order to distribute entangled states over long distances. In recent years, quantum repeaters have become the subject of active theoretical and experimental research, which is reflected in a number of reviews [55–62]. To date, there have been no examples of the implementation of quantum networks based on quantum repeaters, which is primarily due to the lack of effective long-lived quantum memory devices. Efficient operation of quantum repeaters also largely relies on sources of entangled light states and quantum frequency converters, as well as on the possibility of implementing multiplexing, entanglement purification (distillation), and quantum error correction. All this makes the development of quantum repeaters a rather complex task, solving which requires, among other things, fundamental research.

This review describes the operating principles of quantum repeaters, the key device of a full-scale quantum network, and presents an analysis of the existing situation in the field of long-range quantum communication systems. We also consider the current and most promising approaches to designing the main components of quantum repeaters, including quantum memory, sources of nonclassical states of light, and quantum frequency converters.

2. Operating principles of quantum repeaters

When use is made of quantum repeaters, a long communication line is divided into short elementary segments, within which it is still possible to transmit quantum states of light without significant losses, and the entangled quantum state is distributed between the end nodes using such protocols as entanglement swapping [63], entanglement purification [64, 65], and error correction [66, 67]. These protocols no longer require the transmission of quantum states over long distances, but imply the storage of information in quantum memory devices located at intermediate nodes. The main task is to distribute the entangled state between the end nodes of the chain at a rate exceeding the limit of direct transmission. According to fundamental theory, the maximum rate of entanglement distribution or key distribution that can be reached using quantum repeaters is determined by the end-to-end capacity [68],

$$C(\eta, N) = -\log_2\left(1 - \sqrt[N+1]{\eta}\right), \tag{1}$$

where η is the transmissivity of the entire optical line, N is the number of intermediate nodes (insert repeaters), and $N+1$ is the number of elementary segments (lossy channels). In the case of large losses, when $\eta \ll 1$, $C(\eta, N) \approx 1.44\sqrt[N+1]{\eta}$. The quantity $C(\eta, 0) = -\log_2(1-\eta) \approx 1.44\eta$ corresponds to the limit of direct transmission and is known as the Pirandola–Lorenza–Ottaviani–Banchi bound (PLOB bound) [69]. In particular, $\eta = \exp(-L/L_{\text{att}})$, where $L_{\text{att}} \approx 22$ km for a standard fiber with a loss of 0.2 dB km^{-1}. Thus, if the number N of insert repeaters increases proportionally to the total channel length L, the end-to-end capacity will no longer decrease exponentially with increasing distance, but will be determined by the transmission of only an elementary segment, the length of which is fixed.

2.1 Basic protocols

Let us consider some basic protocols that underlie the operation of various schemes of quantum repeaters.

2.1.1 Bell measurement. Measurement in the Bell-state basis is a key element of several quantum communication and quantum computing protocols, such as quantum teleportation [70] and one-way computation [71]. The deterministic version of the Bell measurement involves the implementation of a single-qubit Hadamard element and a two-qubit CNOT element, so that four Bell states at the input,

$$\begin{aligned} |\Phi^{\pm}\rangle &= \frac{1}{\sqrt{2}}\left(|00\rangle \pm |11\rangle\right), \\ |\Psi^{\pm}\rangle &= \frac{1}{\sqrt{2}}\left(|01\rangle \pm |10\rangle\right), \end{aligned} \tag{2}$$

correspond to four measurement results in the computational basis (Fig. 1a). Examples of the implementation of photonic two-qubit elements are available in Refs [72–74]. Nondeterministic versions can be implemented much more simply within the framework of linear optical schemes, among which the most well known are those for single-photon qubits in polarization, time, and Fock bases (see Fig. 1). The first two variants are examples of dual-rail encoding when the states of the computational basis $|0\rangle$ and $|1\rangle$ correspond to two orthogonal modes of the electromagnetic field. In the first case, they correspond to two basis states of linear polarization (horizontal $|H\rangle$ and vertical $|V\rangle$ (Fig. 1b)); and in the second case, to two time windows or modes (time-bin encoding) (the first (early) $|e\rangle$ and the second (late) $|l\rangle$ (Fig. 1c)). The third variant corresponds to single-rail encoding when the states of the computational basis differ in the filling number of one mode: the vacuum state $|0\rangle$ and the single-photon state $|1\rangle$ (Fig. 1d). Regardless of the basis in use, Bell measurements within the framework of linear optics make it possible to determine only two of the four Bell states, so that the overall efficiency of the scheme does not exceed $1/2$ [75]. A higher efficiency can be achieved using linear optical schemes and multiphoton encoding. Thus, when use is made of a logical qubit consisting of $2N$ photons and detectors that resolve states with the number of photons $|0\rangle$, $|1\rangle$, and $|\geqslant 2\rangle$, the

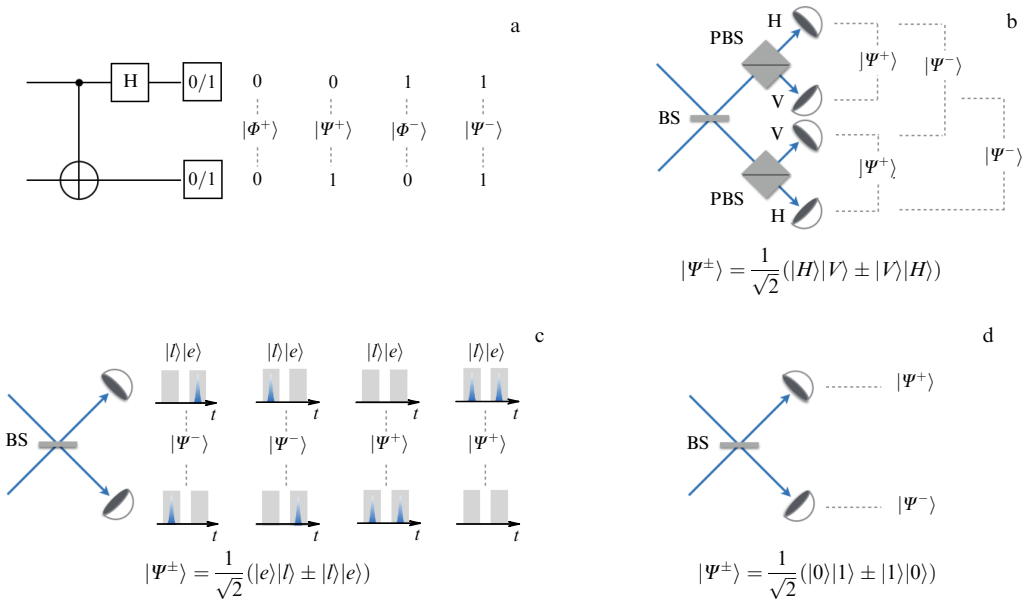

Figure 1. Examples of Bell measurement methods: (a) full deterministic measurement (based on two-qubit CNOT gate) of one-qubit Hadamard gate and projection measurement of qubits, (b) two-photon Bell measurement for entangled states in polarization basis, (c) two-photon Bell measurement for entangled states in time basis, and (d) single-photon Bell measurement for entangled states in Fock basis. Measurement efficiency is 1 in (a) and 1/2 in all other variants, since they allow only two of four states to be distinguished. In (b) and (c), this requires a certain combination of photon count coincidences, as shown by dashed lines, while in (d), a count on only one of two detectors is needed (BS is beam splitter; PBS is polarizing beam splitter; $|H\rangle$ and $|V\rangle$ are single-photon states with orthogonal linear polarization; $|e\rangle$ and $|l\rangle$ are single-photon states with different time delays; and $|0\rangle$ and $|1\rangle$ are vacuum and single-photon states, respectively).

probability of a successful Bell measurement increases to $1 - 2^{-N}$ [76].

2.1.2 Entanglement swapping. The entanglement swapping protocol [63] is a variant of quantum teleportation and allows an entangled state of two qubits to be produced without their direct interaction. Let us consider this protocol in the context of a linear quantum network consisting of three nodes (Fig. 2). Let the entangled states $|\Psi^+_{AC_1}\rangle$ and $|\Psi^+_{C_2B}\rangle$ be distributed between nodes A and C and C and B, respectively. Then, at the intermediate node C, a Bell measurement is performed with qubits C_1 and C_2, which, in the case of a deterministic measurement, yields four possible results. The measurement result is transmitted to one of the end nodes, for example, to node B, where a single-qubit transformation U_B is performed with the qubit located there, the type of which depends on the obtained result. Thus, the maximally entangled state $|\Psi^+_{AB}\rangle$ is distributed between nodes A and B, despite the fact that qubits A and B did not directly interact with each other. Obviously, the entanglement swapping protocol can be viewed from a recursive point of view as a way to successively increase the 'length' of the entangled pair, which forms the basis of a two-way quantum repeater (see Section 2.2).

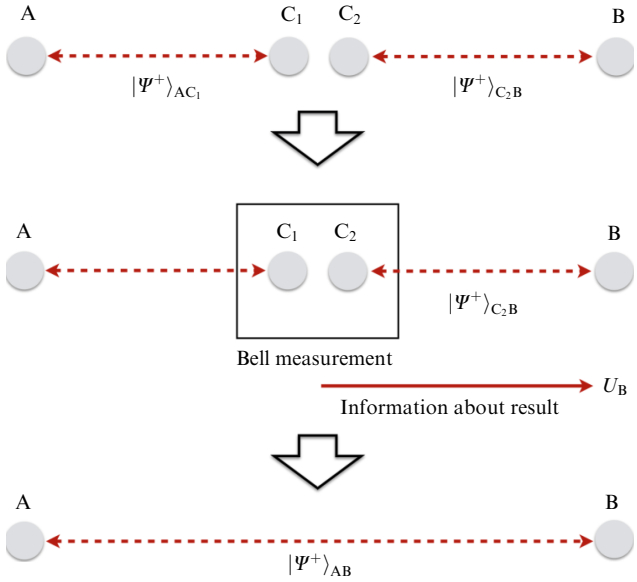

Figure 2. Schematic of entanglement swapping protocol (see explanations in text).

2.1.3 Entanglement purification (distillation). To date, a number of entanglement purification schemes have been proposed (see the review [77]), the most well known of which are those by Bennett et al. [64] and Deutsch et al. [65]. It is also worth mentioning the entanglement pumping scheme proposed in [53, 54]. Let us consider the first scheme as an example, representing imperfectly entangled states as Werner states [78]:

$$\rho = \frac{4F-1}{3}|B\rangle\langle B| + \frac{4(1-F)}{3}I, \qquad (3)$$

where $|B\rangle$ is one of the Bell states, F is the quality (accuracy) of the state, and I is the unit operator in the state space of two qubits. The procedure can be carried out repeatedly in a recursive manner. At each step, use is made of two copies of the entangled state, which are distributed between two nodes (Fig. 3). Within each node, the CNOT operation ($U = I$ transformation) is applied to the qubits of these states. Then, the states of the qubits that played the role of controlled ones are measured in the computational basis $|0\rangle$, $|1\rangle$, and the measurement results are transmitted over the classical channel connecting the nodes. If the results are the

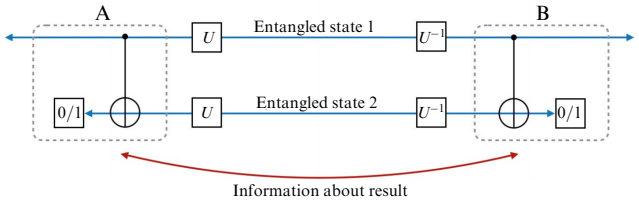

Figure 3. General schematic of heralded entanglement purification (see explanations in text).

same, the purification procedure is considered successful, and one state with a higher quality is obtained, provided that the original quality of the states exceeds 50%. If the measurement results are different, the purification protocol fails, and it is necessary to start over with new entangled states. Thus, a heralded entanglement purification scheme is implemented, the recursive application of which allows one state with high quality to be produced from a set of pairs of entangled states. Recursive formulas describing the probability of success and the quality of the resulting states are given in [53].

The protocol proposed by Deutsch et al. [65] works in a similar way, but, in this case, before performing CNOT operations on each side, single-qubit transformations $U = \begin{pmatrix} 1 & -\mathrm{i} \\ -\mathrm{i} & 1 \end{pmatrix}/\sqrt{2}$ are added, which allows entanglement to be purified not only in the case of the Werner state, but also in the case of an arbitrary two-qubit state of the form

$$\rho = A|\Phi^+\rangle\langle\Phi^+| + B|\Phi^-\rangle\langle\Phi^-| + C|\Psi^+\rangle\langle\Psi^+| + D|\Psi^-\rangle\langle\Psi^-|. \quad (4)$$

2.1.4 Quantum error correction. The development of quantum error correction methods (see reviews [79–81]) is an urgent problem in the field of quantum computing, and the level at which they can be mastered is currently called the era of noisy intermediate scale quantum (NISQ) devices [82, 83]. The main idea is to use a system with redundant state space dimensionality, for example, several physical qubits, and to encode a single logical qubit in such a way that errors can be detected and corrected. Most quantum error correction schemes involve the following steps: (i) encoding a logical qubit through the entangled state of many physical qubits, (ii) determining the type and location of the error by entangling the qubit system with additional qubits and then measuring the additional qubits (finding the error syndrome), and (iii) correcting the error. The first and one of the best known quantum error correction codes is the Shor code [66], in which a logical qubit is encoded as an entangled state of nine physical qubits. Much attention is currently being paid to the development of various versions of topological codes that are more robust to local errors due to the use of the global (topological) properties of the encoding structure, which has the form of a two-dimensional or three-dimensional lattice of qubits (see review [81]). Of particular interest is also the development of encoding methods through the states of a harmonic oscillator (bosonic encoding), when a large dimensionality of the state space is achieved within one degree of freedom of the physical system, which can significantly simplify the experimental implementation (see review [80]). Thus, using the example of a quantum repeater of two elementary segments, Chelluri et al. [84] have recently considered the possibilities of using bosonic quantum error correction to suppress memory loss errors. From the point of view of quantum communication, of great interest is the correction of errors in cluster photon states by performing single-qubit or dual-qubit measurements [85–88], which forms the basis of second- and third-generation quantum repeaters (see Section 2.2). In general, deterministic error correction schemes make it possible to combat both state distortions and qubit losses, but the probability of the latter should not exceed 50%.

2.1.5 Generation of entangled states between quantum memory devices. From the point of view of quantum communication, an important task is to generate entangled states between two stationary qubits or quantum memory devices without their direct interaction. In this regard, several methods have been proposed, oriented towards single atoms [89–95], including superconducting qubits [96], and towards atomic ensembles [97–104] with heralded entangled states, which is important for applications in quantum repeater schemes.

As an example, we consider three schemes (Fig. 4) based on entanglement swapping, in which sources of single-photon or two-photon states are used (see review [55]). In the first one (Fig. 4a), the sources emit pairs of photons in an entangled state, so that one of the photons is immediately stored in the memory device, and the second is transmitted to the central unit, where a two-photon Bell measurement is performed, the scheme of which, as noted above, depends on the qubit encoding. If successful, an entangled state of two quantum memory devices is generated in the corresponding basis. Since storage of one of the photons in the memory means creating a correlation between the remaining photon and the atomic system, this method can be implemented without using two-photon sources if there is a possibility of directly generating an entangled state of the field and the atomic system, as proposed in [90–92]. In the second scheme (Fig. 4b), the sources emit pairs of photons in a factorized state, which are also sent to the quantum memory devices and the central unit, where a one-photon Bell measurement is performed. If successful, an entangled state of two quantum memory devices is generated in the Fock basis. This scheme, unlike the first one, can be used only with probabilistic two-

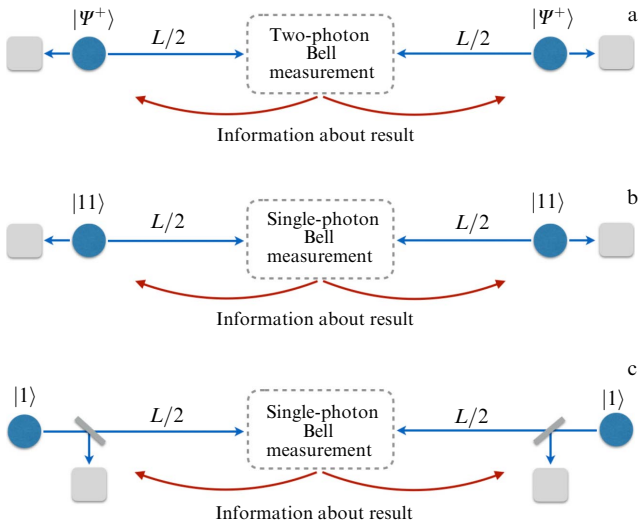

Figure 4. Examples of methods for generating entanglement between two quantum memories (gray squares) based on entanglement swapping using sources of (a) two-photon entangled, (b) two-photon factorized, and (c) single-photon states.

Table 1. Heralded probability and success probability of entanglement generation for schemes based on entanglement swapping (see Fig. 4).

Generation scheme	Heralded probability	Success probability
Two-photon source and two-photon Bell measurement (Fig. 4a)	$\eta_s^2\eta_t^2\eta_d^2/2$	$\eta_s^2\eta_t^2\eta_d^2/2$
Two-photon source and single-photon Bell measurement (Fig. 4b)	$2\eta_s\eta_t\eta_d(1-\eta_s\eta_t\eta_d)$	$2\eta_s\eta_t\eta_d(1-\eta_s)$
Single-photon source and single-photon Bell measurement (Fig. 4c)	$2\gamma\eta_s\eta_t\eta_d(1-\gamma\eta_s\eta_t\eta_d)$	$2\gamma\eta_s^2\eta_t\eta_d(1-\gamma)$

Notations: η_s is source efficiency, $\eta_t = \eta_{L/2}$ is transmission of channel between source and central unit, η_d is detector efficiency, and γ is probability of photon passing through beam splitter. In all cases, it is assumed that photon-number resolving detectors are used.

photon sources, which significantly limits the entanglement generation rate. At the same time, it is equivalent to the well-known Duan–Lukin–Cirac–Zoller (DLCZ) scheme [97] (see Section 3.1), in which similar correlations are created using radiative quantum memory. Finally, the third scheme (Fig. 4c) uses sources of single photons, which with some probability either are reflected from the beam splitter and enter the quantum memory or pass through the beam splitter and are directed to the central unit, where a single-photon Bell measurement is performed. Therefore, as in the second scheme, an entangled state of two quantum memory devices in the Fock basis is generated; however, the maximum generation rate is achieved with deterministic photon sources. Table 1 contains formulas describing the heralded probability and the success probability of entanglement generation in the described schemes. The ratio of the success probability to the heralded probability determines the conditional efficiency of generation or the quality of the prepared state. For two- and single-photon Bell measurements, the heralded probability is defined as the probability of detecting a single-photon state at each detector and at one of the two detectors, respectively. In the second case, the success probability only takes into account those events when only one photon enters the Bell measurement unit from either side.

It is important to note that the entangled state in the Fock basis, which corresponds to the distribution of single-photon excitation between two quantum memory devices, has limited application, since it is difficult to perform measurements in bases other than the Fock basis. Therefore, to produce a two-photon entangled state, one more step is needed, namely, post-selection of this state using two pairs of quantum memories with single-photon entanglement [97]. Another approach to generating a two-photon entangled state, recently proposed in [105], is based on post-matching of single-photon measurements (see Section 2.3).

The above schemes assume that the Bell measurement is performed at an intermediate station between the nodes, each of which contains a memory device and a photon source (or emitting memory). Other options are also possible: when the Bell measurement is localized in one of the nodes or when a source of photon pairs is placed between the nodes and the Bell measurement is performed at each node. A comparative analysis of such schemes can be found in [106, 107].

An alternative approach is nonlocal schemes that use an additional photon, which first sequentially interacts with two

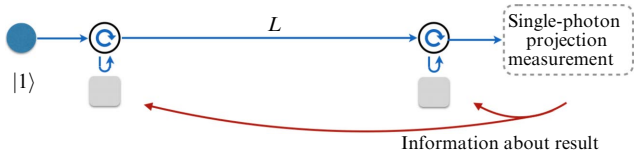

Figure 5. Schematic diagram of generating entanglement between two atoms in cavities (gray squares) using a source of single photons (blue dot), which sequentially interact with cavities via optical circulators (circles with circular arrows) and are directed to a unit where a projection measurement of a single-photon qubit is performed.

memory cells (atoms in cavities) and then is detected. The measurement result is reported to perform local transformations, as a result of which a nonlocal logical element is implemented, for example, CNOT, or an entangled state of two memory devices is generated [43, 108–110] (Fig. 5). In this case, the main scheme for the interaction of a photon with an atom in a cavity is the CNOT operation between an atomic qubit and a photon qubit, implemented when a photon is reflected from the cavity [111, 112]. Finally, an entangled state of two atoms can be generated using the effect of heralded photon absorption [113], which is a promising development of the known scheme for transferring a quantum state from one atom to another [114, 115] (see Section 3.1).

Various schemes for generating (both heralded and unheralded) entanglement for the general case of a multi-node quantum network are reviewed in [116].

2.2 Main types of quantum repeaters

Quantum repeater protocols are usually divided into two categories: *two-way quantum repeaters* and *one-way quantum repeaters*. The first is based on probabilistic heralded entanglement generation between neighboring intermediate nodes (Fig. 6). Once an entangled state is successfully generated on a segment, it is stored in the local quantum memory until an entangled state is produced on a neighboring segment. After that, an entanglement swapping protocol is performed, which leads to its distribution over a larger distance. The procedure is repeated until the entangled state is distributed between the end nodes. The entanglement swapping protocol helps eliminate photon losses in quantum channels, but it is still necessary to combat the distortions of quantum states that arise during their generation, transmission, and transformation. This can be done by using a probabilistic heralded entanglement purification protocol, which allows many low-precision Bell pairs to be converted into fewer, higher-precision states, implying two-way classical communication between nodes. The combined use of probabilistic heralded entanglement generation and purification protocols is the basis of *first-generation quantum repeaters* [53, 54, 95, 97–104, 117–122]. The need for two-way heralding within the entire communication link, at least for purification protocols, is the main factor limiting the rate of entangled state generation between end nodes; moreover, it places the highest demands on the storage time of quantum states at intermediate nodes. In the worst case, entanglement purification has to be performed at the scale of the entire chain of quantum repeaters, which slows down the achievable repetition rate to values on the order of c/L, where $c \approx 2.14 \times 10^8$ m s^{-1} is the speed of light in fiber. To avoid this slowdown, quantum error correction can be used instead of heralded entanglement purification,

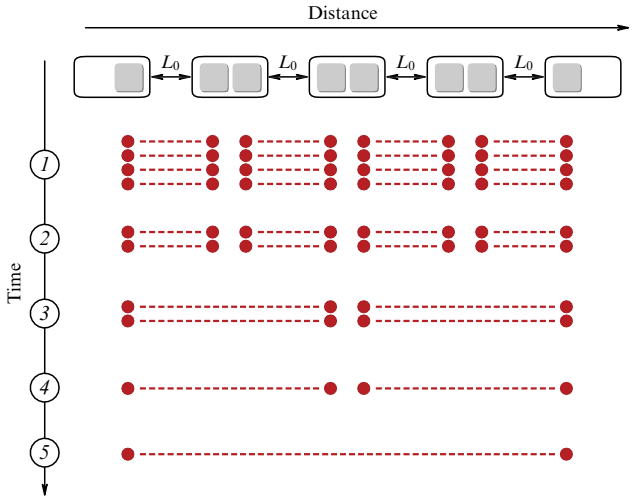

Figure 6. Schematic diagram of distributing entangled state using two-way quantum repeater. Upper line depicts communication link divided into four elementary segments and containing three intermediate nodes, each of which has two memory devices (gray squares). Protocol starts with (*1*) generating a set of entangled qubit pairs (red dots connected by dotted line) within each elementary segment, then (*2*) performing entanglement purification, and (*3*) swapping first-level entanglement via Bell measurement at second and fourth intermediate nodes. Next, (*4*) entanglement purification and (*5*) second-level entanglement swapping are performed via Bell measurement at central node. Each step is probabilistic and is repeated until success is achieved, information about which is transmitted between nodes via heralded signals.

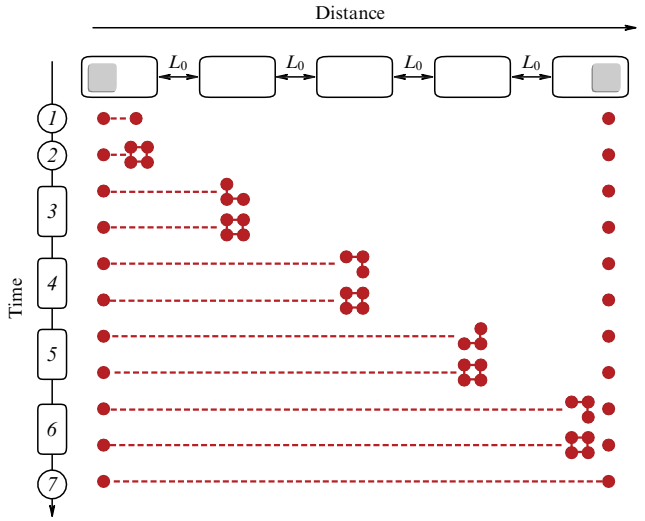

Figure 7. Schematic diagram of entangled state distribution using one-way quantum repeater. Upper line depicts chain of repeaters divided into four elementary segments and containing three intermediate nodes, which may or may not have memory devices (gray squares). Protocol begins with generation of entangled pair of qubits (red dots connected by dotted line), (*1*) one of which is written to quantum memory and (*2*) the other is encoded via a multi-qubit logic state. (*3–6*) Multi-qubit state is then sequentially transmitted to neighboring nodes, where error correction is performed due to both loss of qubits and degradation of state quality. Finally, at the last node, (*7*) logical state is transferred to qubit in final memory device.

resulting in *second-generation quantum repeaters* [86, 123–127].

In this case, two-way heralding is required only between adjacent nodes, and so the upper bound on the repetition rate is now determined by the ratio c/L_0, which gives a value of about 1 kHz for $L_0 \sim 100$ km. Even higher repetition rates can be achieved by abandoning two-way heralding altogether and using quantum error correction to combat both losses and state distortions. This approach is implemented in one-way quantum repeaters or *third-generation quantum repeaters* [85, 87, 88, 128–139]. In this case, quantum information is encoded via multiphoton logical qubits and transmitted directly over noisy channels (Fig. 7). If the error rate is below the noise immunity threshold, the damaged logical qubits are restored at the nodes by quantum error correction and transmitted from node to node until they reach the end point. As a result, the repetition rate is limited only by the rate of state preparation, local operations, and measurements at intermediate nodes. Moreover, the entire scheme can be implemented even without quantum memory devices [85, 140]. However, each individual node must contain a small-sized quantum computer for error correction. In addition, in the case of a third-generation quantum repeater, the loss in each section must be less than 3 dB (50%) to implement deterministic error correction (which corresponds to the general theory regarding the possibility of one-way quantum communication [141]), and so the distance between nodes should not exceed 15 km (for a standard fiber with a loss of 0.2 dB km^{-1}). As a result, taking into account other losses such as input/output losses from memory devices, it is necessary to place nodes every few kilometers along the entire communication line [129]. A more detailed discussion of the different generations of quantum repeaters is presented in reviews [55, 57, 60, 142].

2.3 Analysis of first-generation quantum repeaters

We will consider in more detail first-generation quantum repeaters. Let an extended communication line of length L be divided into 2^n elementary segments of the same length L_0 ($L = L_0 \times 2^n$). We introduce the following parameters: p_g is the probability of successful generation of an entangled state within an elementary segment, and p_s is the probability of successful entanglement swapping. The main task of statistical analysis is to estimate the average number of attempts N_n required to distribute the entangled state between the end nodes of the chain. In some cases, this value can be calculated analytically, but, in the general case, it is possible to estimate only its lower and upper bounds (Table 2).

Since the number n of entanglement swapping levels (the degree of protocol nesting) depends on the number of segments only logarithmically, the fundamental point is the dependence $N_n \propto 1/p_g$, where p_g increases with decreasing length of the elementary segment. In particular, for the three variants of entangled state generation via Bell measurement, considered in Section 2.1, we have $p_g \propto \eta_{L_0/2}^2 = \exp(-L_0/L_{att})$ and $p_g \propto \eta_{L_0/2} = \exp(-L_0/2L_{att})$ in the case of two-photon and one-photon Bell measurements, respectively. Thus, for a fixed value of L, the average number of attempts required to distribute the entangled state between the end nodes decreases with increasing number of segments, demonstrating an exponential speedup compared to direct transmission.

Having estimated the average number of attempts, one can estimate the average waiting time and the rate of entanglement distribution. The simplest approach is to define the average waiting time as $T_n = N_n T_c$, where T_c is the minimum time interval between attempts to generate a heralded entangled state within an elementary segment (see [60, 61]). This approximation works well if the purifications

Table 2. Estimates of average number of attempts, N_n, required to distribute entangled state within 2^n elementary segments.

Estimates of average number of attempts	Applicability conditions	Literature
$N_1 = \frac{1}{p_s}\frac{(3-2p_g)}{(2-p_g)}\frac{1}{p_g}$		[55, 60, 143, 144]
$N_n = \sum_{j=1}^{2^n}\binom{2^n}{j}\frac{(-1)^{j+1}}{1-(1-p_g)^j}$	$p_s = 1$	[145, 146]
$N_n \approx \left(\frac{3}{2p_s}\right)^n \frac{1}{p_g}$	$p_g \ll 1, p_s \ll 1$	[55, 144]
$\frac{1}{p_s}\left(\frac{3-2p_s}{2p_s(2-p_s)}\right)^{n-1}\frac{3-2p_g}{p_g(2-p_g)} \leqslant N_n$ $N_n \leqslant \left(\frac{3}{2p_s}\right)^n\left[1-\frac{1}{\ln(1-p_g)}\right]$		[147]

Notations: p_g is probability of successful generation of entangled state within elementary segment, and p_s is probability of successful entanglement swapping.

protocols are applied only at the level of elementary segments. In the above-mentioned schemes for generating heralded entanglement, $T_c = L_0/c$, which is equal to the sum of the photon propagation time from a node to the central beam splitter and the return propagation time of the heralded signal from the central beam splitter to the node. Then, the rate of the entangled state distribution, which can be defined as $1/T_n$, turns out to be proportional to

$$\sqrt[N+1]{\eta(L)} = \exp\left(-\frac{L_0}{L_{att}}\right)$$

in the case of a two-photon Bell measurement or to

$$\sqrt[N+1]{\eta(L/2)} = \exp\left(-\frac{L_0}{2L_{att}}\right)$$

in the case of a single-photon one, where N is the number of intermediate nodes, and $N+1 = 2^n$ is the number of elementary segments, which agrees with the fundamental limit for the end-to-end capacity (1).

Note that the use of a single-photon Bell measurement allows one to achieve a distance twice as large as the two-photon version at the same generation rate, but this requires stabilization of the optical length of the channel to observe stable interference, which is a technically challenging task for large distances. Li et al. [105] proposed a scheme of a repeater based on an asynchronous two-photon Bell measurement [148, 149] by post-matching two successful single-photon measurements, which makes it possible to overcome this drawback: to achieve scaling of the form $\exp(-L_0/2L_{att})$, without high-precision stabilization of the optical length.

A fundamental point is to take into account relaxation in quantum memory devices. Wu et al. [150] considered the simplest case with two elementary segments, for which analytical estimates can be obtained. In particular, it follows from the results of the theory that, for a given entanglement distribution rate, a decrease in the memory efficiency can be compensated within certain limits by increasing the storage time and vice versa. For example, when use is made of an entanglement generation scheme with deterministic two-photon sources (Fig. 4a) and a total system length of 100 km, the entangled state generation rate can reach units of Hz, provided that the memory efficiency exceeds ~ 0.5 (~ 0.65), and the storage time is no less than ~ 10 ms (~ 1 ms). In any case, the storage time in quantum memory determines the maximum length of the communication line, at which the presence of an intermediate repeater node provides an advantage in rate compared to direct transmission. As the number of segments increases, the situation becomes more complicated, since the total storage time in quantum memory devices, which determines the efficiency of the protocol, depends on the order of entanglement generation and swapping operations, so that optimization of the entire scheme becomes important [151, 152]. A detailed analysis of this issue for a small number of nodes and deterministic entanglement exchange is given in [153], where, in particular, it is shown that the optimal strategy is a dynamic exchange order, in which entanglement swapping is performed in any order as segments become ready (the 'swap as soon as possible' method).

Analysis of the influence of losses in quantum repeater nodes on the maximum quantum communication rate is presented in [154]. Examples of numerical calculations of entanglement distribution using quantum repeaters with entanglement purification taken into account can be found in [144, 155, 156]. The general conclusion is that, for the efficient operation of a first-generation quantum repeater, the information storage time in quantum memory devices should exceed the propagation time of optical signals between the end nodes of the chain [157]. On the other hand, this time determines the maximum repetition rate of entanglement distribution attempts when using the purification protocol, which significantly reduces the distribution rate over large distances. A promising approach to solving the problem is multiplexing. Its various schemes are proposed in [95, 98, 124, 143, 158–164], which involves the development of corresponding multimode or multi-qubit quantum memory devices (see Section 3.3). At the same time, beyond the PLOB bound, an increase in the repeater rate due to multiplexing of M channels is practically equivalent to an increase in the rate due to an increase in the coherence time of quantum memory by M times [153]. Another resource for increasing the efficiency of quantum repeaters is the transition to deterministic entanglement swapping schemes [95, 117, 165, 166], the development of which is also an important research task.

3. Basic devices of quantum repeaters

3.1 Comparative analysis of main quantum memory schemes

Quantum memory, which acts as a controlled delay line for quantum states of the electromagnetic field, is a key component of quantum repeaters and allows probabilistic processes to be synchronized at different stages of the distribution of entangled states. The main parameters of quantum memory include the following:

• Efficiency. It is defined as the ratio of the output pulse energy to the input pulse energy or as the probability of retrieving a single-photon state. Efficiency is usually determined for the minimum storage time, which is actually limited from below by the duration of the input light pulse.

• Fidelity or quality. In the general case, a quantum memory device converts the input state of the electromagnetic field, described by the density matrix ρ_{in}, into some

output state, which is described by another density matrix ρ_{out}. The accuracy of retrieving the original state, or the quality of quantum memory, is defined as

$$F = \left(\text{Tr} \sqrt{\sqrt{\rho_{\text{in}}}\, \rho_{\text{out}} \sqrt{\rho_{\text{in}}}} \right)^2 .$$

For a memory device in which single photons are stored and retrieved, the fidelity is defined as the correlation of the amplitudes of the input and output single-photon wave packets. It is called conditional fidelity, since it arises due to the re-emission of a photon and is independent of the efficiency. The maximum fidelity equal to unity (or 100%) is realized for the case of complete coincidence of the quantum states of the light pulses stored in and retrieved from the quantum memory.

• Storage time. For quantum communication through quantum repeaters, a fundamentally important parameter is the storage time of quantum states, which is defined as the time during which the memory efficiency decreases by a factor of e (or two times) relative to the maximum value achieved at a minimum storage time. According to this definition, the storage time is two times shorter than the decoherence time, which determines the drop in the field amplitude (by the corresponding number of times) at the device output.

• Mode capacity. This parameter is defined as the number of electromagnetic field modes that can be stored and retrieved with the required fidelity and efficiency. In the general case, the mode functions of the field are specified by polarization, frequency, time, and spatial degrees of freedom. Notably, the mode capacity in the time domain is determined by the maximum ratio of the storage time to the input pulse duration, which coincides with another important parameter of quantum memory—the time bandwidth product (TBP).

Ideal quantum memory is characterized by unit fidelity, unit efficiency, infinite storage time, and infinite mode capacity. Currently, the main problem on the way to ideal quantum memory is the combination of high values of these parameters in a single device. From this point of view, quantum memory can be called the main locking technology in the field of long-range quantum communication.

The efficiency of first-generation quantum repeaters significantly depends on the possibility of using multiplexing methods. Therefore, much attention is currently being devoted to the development of quantum memory devices based on polyatomic ensembles that allow various quantum states of the electromagnetic field, in particular single-photon wave packets, to be stored and retrieved in the multimode regime, thereby implementing high-order multiplexing. On the other hand, multiqubit quantum memory, which is essentially a quantum register, makes it possible to combine long-term storage of information with the execution of quantum operations, such as quantum error correction or deterministic Bell measurement.

Various quantum memory schemes are described in a number of reviews [167–176]. In addition to dividing the proposed schemes into the two classes mentioned above (multimode memory based on atomic ensembles and multiqubit memory based on quantum registers), a distinction is also made between absorbing and emitting quantum memory. The first case implies storing and retrieving quantum states of light coming from outside; therefore, such devices are also called write/read memory. In the second case, quantum memory is combined with a photon source, so that emission from the latter indicates the transfer of quantum memory to a superposition state, which is equivalent to writing information. This memory is also called 'write-only memory' or 'heralded memory.'

From the point of view of quantum repeaters and quantum networks, of interest are long-lived quantum memory devices. As a rule, two elements can be distinguished in such devices: an information carrier with a long coherence time but that weakly interacts with the field, and an interface that interacts well with the field and acts as an intermediary between it and the carrier. In this regard, there are two basic options: multilevel and multiparticle. For example, in the case of a polyatomic ensemble, the presence of a Λ-type energy level structure is usually assumed, where one of the optical transitions is used to absorb/emit photons (interface), and the low-frequency transition is used to store information (carrier). This is a multilevel scheme. In the case of multiqubit memory, the second option is obviously also possible: the memory cell consists of two interacting particles, one of which interacts well with the field (qubit for communication), and the second has a long coherence time (qubit for memory). However, the second option is also possible for ensembles, such as a mixture of two atomic gases, where one type of atom is used for bonding (alkali metal atoms) and the other is used for storage (noble gas atoms). Below, we consider the main quantum memory schemes that are most actively used in experiments and exemplify the above-mentioned varieties. A detailed analysis of theoretical models of quantum memory can be found in review [172].

3.1.1 Electromagnetically induced transparency. Electromagnetically induced transparency (EIT) is a quantum interference effect that can be observed in a multilevel atomic system, where the interference of two different excitation paths results in a narrow transparency window within the atomic absorption spectrum [177, 178]. The atoms are assumed to have a Λ-type energy level structure, as shown in Fig. 8, and interact with a strong control field at one of the optical transitions. The action of the control field is equivalent to the opening of a gap (transparency window) in the absorption spectrum of the atoms at the frequency of the probe field, the width of which is proportional to the intensity of the control field and inversely proportional to $\sqrt{d}$, where d is the optical thickness of the sample for the probe field. The probability of transition from the ground state $|g\rangle$ to the excited state $|e\rangle$ under the action of the probe field is inhibited due to destructive interference between the probability amplitudes of the two transition paths: $|g\rangle \to |e\rangle$ and $|g\rangle \to |e\rangle \to |s\rangle \to |e\rangle$ [177].

If the frequency of the probe pulse is inside the transparency window, the probe pulse undergoes strong normal dispersion, which leads to a decrease in the group velocity of light. So-called 'slow light' arises, the group velocity of which is proportional to the intensity of the probe field. In this case, a state appears binding the probe field acting at the $|g\rangle \to |e\rangle$ transition with the polarization of the medium at the $|g\rangle \to |s\rangle$ transition, a so-called dark polariton. A remarkable feature of the dark polariton is the possibility of complete transfer of the field energy into coherence at the low-frequency transition $|g\rangle \to |s\rangle$ when the control field is switched off and the group velocity is reduced to zero. This effect is the basis of quantum memory (see Fig. 8) [179, 180]. The general procedure for storing and retrieving weak light pulses (in particular, single-photon ones) is as follows.

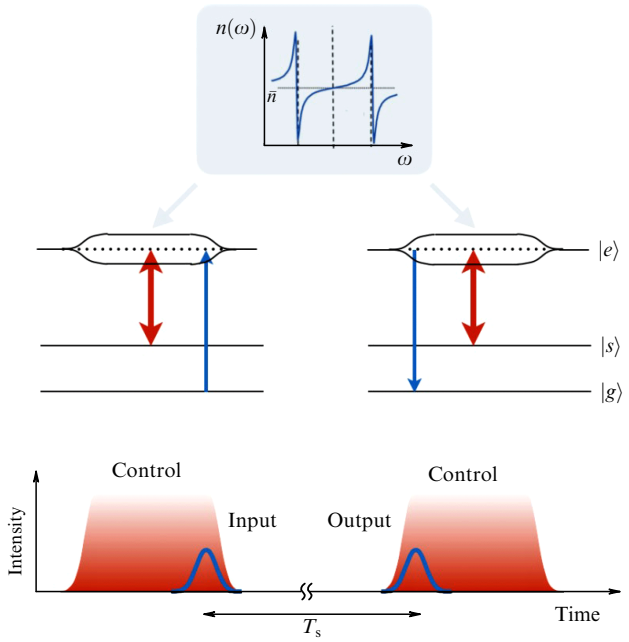

Figure 8. Illustration of operating principle of EIT-based quantum memory (see explanations in text): $n(\omega)$ is refractive index of medium near transition frequency $|g\rangle \rightarrow |e\rangle$ with control field turned on, and T_s is information storage time on long-lived transition $|g\rangle \rightarrow |s\rangle$.

First, all the atoms are prepared in the ground state $|g\rangle$ using optical pumping, so that the initial state of the atomic ensemble takes the form $|\phi_0\rangle = |g_1 \dots g_N\rangle$. Then, the control field is switched on, creating a transparency window. During the slow propagation of the probe field in the medium, the control field is switched off, and the atomic ensemble undergoes a transition to a state of collective excitation of the form

$$|\phi_s\rangle = \sum_{j=1}^{N} \phi_j |g_1 \dots s_j \dots g_N\rangle\,, \qquad (5)$$

where N is the total number of atoms, $|g_j\rangle$ and $|s_j\rangle$ are the ground state and the long-lived state of the jth atom, and the amplitude ϕ_j takes into account the difference between the wave vectors of the control and probe fields. This step corresponds to the storage of information. Further switching on of the control field leads to the reverse recovery of the dark polariton, which eventually leaves the medium as a light pulse. The memory time is obviously determined by the relaxation time of the coherence at the low-frequency transition $|g\rangle \rightarrow |s\rangle$.

Since the group velocity of light inside the medium is proportional to the power of the control laser and inversely proportional to the optical thickness d, while the EIT bandwidth or the transparency window width is inversely proportional to $\sqrt{d}$, the TBP value turns out to be proportional to $\sqrt{d}$. Thus, the mode capacity of EIT-based memory is low at typical optical thicknesses, which is the main drawback of this approach. In addition, fluorescence noise may occur, which cannot be filtered out due to its identity with signal photons [181]. On the other hand, the EIT effect can be observed in a wide variety of materials. EIT-based quantum memory has long been realized in gases at room temperature [182], ultracold gases [183], and crystals doped with rare earth ions at helium temperatures [184], with the highest (above 90%) quantum memory efficiencies being achieved in cold atoms in the EIT regime [185].

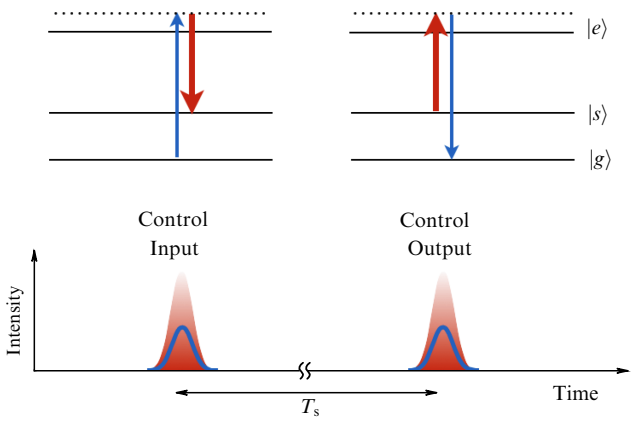

Figure 9. Illustration of operating principle of quantum memory based on off-resonant Raman absorption/emission (see explanations in text): T_s is information storage time on long-lived transition $|g\rangle \rightarrow |s\rangle$.

3.1.2 Off-resonant Raman absorption/emission of photons. This scheme, like EIT, implies the interaction of a strong control field and a weak probe field with a three-level atomic system under Raman resonance conditions; however, neither of these fields is in resonance with optical transitions [186]. It is assumed that the atoms have a Λ-type energy level structure, as shown in Fig. 9, and are prepared in the ground state $|g\rangle$ by optical pumping. The simultaneous action of a weak probe field (photon) and a strong control field leads to the absorption of a photon and the transfer of one of the atoms to the state $|s\rangle$ by stimulated Raman scattering of the control field. As a result, the atomic ensemble undergoes a transition to a collective state that is similar to state (5). The action of the readout pulse leads to the generation of a single-photon state due to spontaneous Raman scattering on the generated atomic coherence.

Compared to EIT, the off-resonant Raman absorption/emission scheme is less susceptible to fluorescence noise and provides the ability to store data with high throughput (storage and retrieval of broadband pulses). However, these advantages are achieved at the expense of a stronger control field, which compensates for the weak coupling under conditions of large single-photon detuning. As a result, the four-wave mixing noise in Raman memory is usually higher than that in EIT-based quantum memory. An effective way to suppress noise is to use a cavity that is resonant with the probe field and anti-resonant with the noise field [187].

The main disadvantage of the scheme in question is the need to match the pulse shape of the write field with that of the probe field to achieve high efficiency. However, combining off-resonant Raman absorption/emission with controlled inhomogeneous broadening [188], for which it is sufficient to use angular modulation of the control field [189, 190], makes it possible to eliminate such synchronization and implement multimode memory in the time domain.

3.1.3 Controlled reversible inhomogeneous broadening. Controlled reversible inhomogeneous broadening (CRIB) is one of the main mechanisms for implementing quantum memory based on a photon-echo approach(see reviews [169, 176]), due to which an atomic system can experience a fully reversible

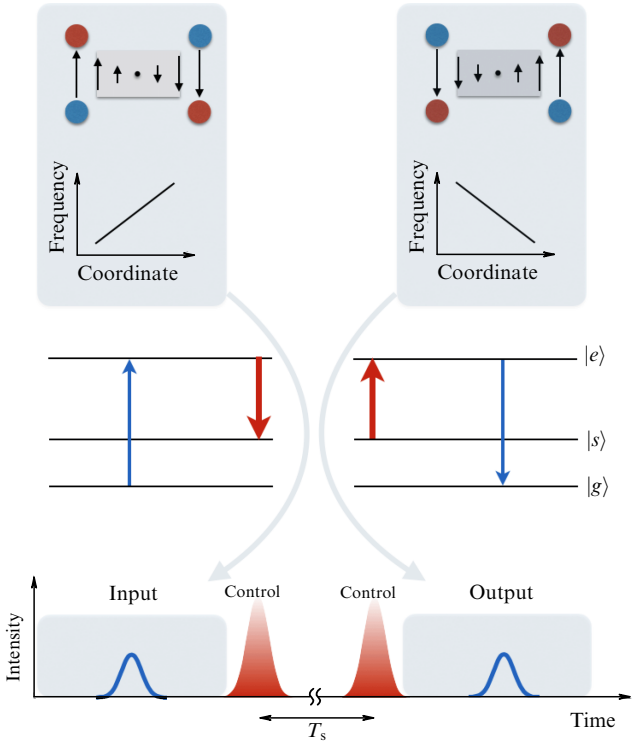

Figure 10. Illustration of operating principle of quantum memory based on gradient photon echo (GEM) (see explanations in text): T_s is information storage time at long-lived transition $|g\rangle \rightarrow |s\rangle$.

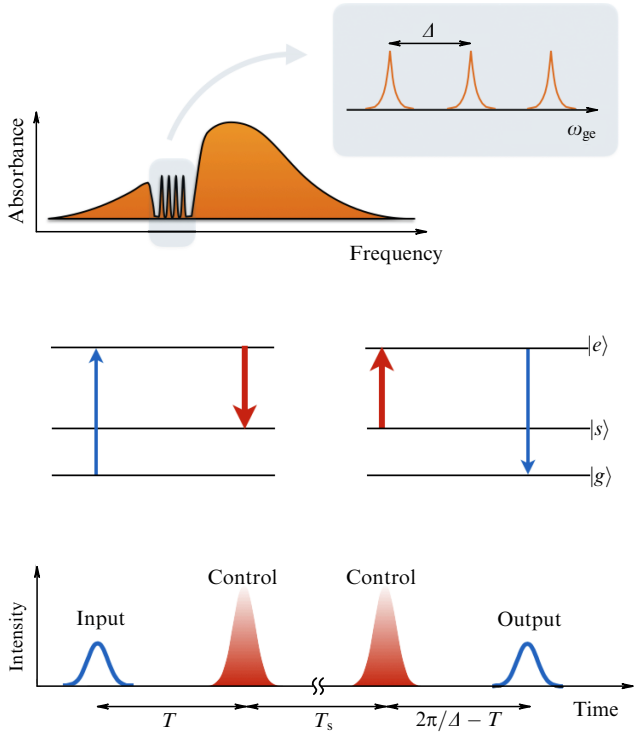

Figure 11. Illustration of operating principle of quantum memory based on atomic frequency comb (see explanations in text): T_s is information storage time at long-lived transition $|g\rangle \rightarrow |s\rangle$, and Δ is frequency comb period.

evolution. This protocol requires the presence or creation of a narrow spectrally isolated absorption line in the atomic ensemble, the inhomogeneous broadening of which can be controlled using an external electric or magnetic field. For example, CRIB can be achieved using an electric field gradient and the linear Stark effect in solids doped with rare earth elements, which have a permanent dipole moment [191, 192]. The cycle of writing and reading the probe field begins with the absorption of the probe field by the broadened line. After absorption, the external field is switched off, which allows the coherence to be transferred to a long-lived spin transition using an optical π pulse. The stored state is retrieved on demand by translating the coherence back to the optical transition and changing the sign of the external field to generate a photon echo. When the direction of propagation of the probe field is parallel to the gradient of the external field, the result is called gradient echo memory (GEM) [193] or the longitudinal version of CRIB (Fig. 10). A distinctive feature of the GEM protocol is its high forward retrieval efficiency [194, 195], since the presence of a longitudinal gradient eliminates reabsorption of radiation in the medium.

It should also be noted that, instead of additional pulses, a method with off-resonant Raman absorption can be used to store information on long-lived spin states [188]. Unlike EIT or Raman memory, whose mode capacitance scales as $\sqrt{d}$, the CRIB protocol is characterized by a mode capacitance that scales linearly with the optical thickness d [196]. The main problem of the protocol is a significant decrease in the optical thickness with the broadening of the initial absorption line.

In the case of transverse CRIB, the storage and retrieval efficiency approaches unity with increasing optical thickness, provided that readout is performed in the opposite direction to the propagation of the input pulse, which is realized using counterpropagating control field pulses. Otherwise, it does not exceed 54% at an optical thickness of about 2. In the case of GEM (longitudinal CRIB), the efficiency approaches unity with increasing optical thickness and with forward retrieval. An alternative method for achieving high efficiency without increasing optical thickness is to use a cavity [197, 198].

3.1.4 Atomic frequency comb. An atomic frequency comb (AFC) is a special case of inhomogeneous broadening of a resonant transition, in which the absorption spectrum has the form of a periodic system of narrow lines. Such a structure can be prepared, for example, in crystals doped with rare-earth ions using spectral hole burning methods, provided that the inhomogeneous broadening Γ_{inh} of the transitions is significantly greater than the homogeneous one Γ_{h}. A distinctive feature of the structure of inhomogeneous broadening is the possibility of periodic phasing of the atomic polarization, similar to the effect of mode locking in a laser cavity, which served as the main idea for the quantum memory protocol proposed and implemented in [199, 200] (Fig. 11). To begin with, in the inhomogeneously broadened absorption profile at the $|g\rangle \rightarrow |e\rangle$ transition, an AFC with some period Δ is generated by transferring atoms to a long-lived auxiliary energy level $|\text{aux}\rangle$ (not shown in the figure) using frequency-selective optical pumping. When such a system interacts with a resonant probe field (photon) at the $|g\rangle \rightarrow |e\rangle$ transition, the field is absorbed and collective atomic excitation is created, which can be written in the form

$$|\phi_{\text{e}}\rangle = \sum_{j=1}^{N} \phi_j \exp\left(\text{i}\delta_j t\right) |g_1 \ldots e_j \ldots g_N\rangle\,, \tag{6}$$

where N is the total number of atoms in the AFC, $|g_j\rangle$ and $|e_j\rangle$ are the ground state and the excited state of the jth atom, δ_j is the laser frequency detuning from the atomic transition frequency, and the amplitude ϕ_j depending on the position of the atoms is determined by the parameters of the light pulse and the AFC.

It is assumed that the spectral width of the photon is limited from below (above) by the distance Δ between the AFC peaks (the total width of the AFC). After a photon is absorbed, different members in the collective excitation state $|\phi_e\rangle$ having different detunings δ_j begin to accumulate different phases. However, due to the periodic structure of the AFC, for which $\delta_j = m_j\Delta$, all members in the state $|\phi_e\rangle$ again acquire the same phase (with an accuracy of 2π) at time $t = 2\pi/\Delta$. This phasing process leads to re-emission of the input photon at time $t = 2\pi/\Delta$, which is interpreted as a retrieval of the recorded state. To implement on-demand readout at the required time, one can use the third long-lived (spin) state $|s\rangle$, transferring coherence from the $|g\rangle \rightarrow |e\rangle$ transition to the $|g\rangle \rightarrow |s\rangle$ transition and back using π pulses of the control field. When coherence is transferred to the $|g\rangle \rightarrow |s\rangle$ transition before photon emission, the dephasing progress is frozen [the ensemble state again has form (5)]. Then, after a time T, the coherence returns to the $|g\rangle \rightarrow |e\rangle$ transition, and the phase evolution continues, so that a photon is emitted when the total time after absorption becomes equal to $T + 2\pi/\Delta$. In this way, it is possible to simultaneously realize the on-demand readout of the single-photon state at the time $T + 2\pi/\Delta$ and to attract the long-lived spin state for storage.

Alternative approaches to on-demand readout include a combination of CRIB and AFC protocols for each absorption line [201] and using the Stark shift to control interference in the atomic ensemble [202–204].

Unlike many other memory protocols, the mode capacity of the AFC is not limited by the optical thickness, which is a major advantage of this protocol [196]. This is because the ratio of storage time to pulse duration, which determines how many time modes can be stored in quantum memory, is independent of the optical thickness, making the AFC a promising candidate for multimode memories. The storage and retrieval efficiency approaches unity as the optical thickness increases, provided that the readout is performed in the direction opposite to the input pulse propagation, which is achieved using counterpropagating control field pulses. Otherwise, it does not exceed 54% at an optical thickness of about 2. An alternative method for achieving high efficiency without increasing the optical thickness is to use a cavity [197, 198], which has recently been used to demonstrate an AFC-based memory efficiency of 62% [205]. We also note paper [206], which reported a 15-fold increase in the memory efficiency in a cavity compared to that in the single-pass regime.

In the context of AFC-based quantum memory, we can also note the recent work by Moiseev et al. [207], who proposed a new quantum memory protocol using coherence created in advance on a long-lived transition. This coherence allows echo signals to be observed at specified times, as is the case of the AFC, but has the advantage of using the entire inhomogeneous absorption linewidth.

3.1.5 Revival of silenced echo. One more interesting approach is the protocol known as revival of silenced echo (ROSE) [208]. In this protocol, optical π-pulses are applied to an unstructured inhomogeneously broadened ensemble to rephase the collective atomic coherence generated by an absorbed single photon pulse. To avoid noise resulting from the inverted atomic population, the first echo is suppressed by the spatial phase mismatch generated by the first optical π-pulse. A second π-pulse with appropriate phase matching transfers the population to the ground state and allows the suppressed echo to be reconstructed. The advantage of the ROSE protocol is that it exploits 'natural' inhomogeneous broadening of the resonant transition, which eliminates the need for preparing narrow absorption lines. In addition, this protocol allows broadband quantum memory to be implemented, since it uses all the potential of the inhomogeneous broadening of the optical transition. Note, however, that an increase in the band leads to a decrease in efficiency [209]. This protocol, despite its attractiveness, requires very precise implementation of π-pulses, and so the possibility of its application in the single-photon regime has not yet been demonstrated.

3.1.6 DLCZ protocol. The DLCZ scheme proposed in [97] is the main one for radiating memory based on atomic ensembles. It is based on the effect of spontaneous Raman scattering of light in a three-level system of atoms. In comparison to memory based on off-resonant Raman absorption, in the DLCZ protocol, instead of converting the input photon into low-frequency atomic coherence, atomic coherence is generated during spontaneous Raman scattering of pump radiation, which is accompanied by the emission of a heralding photon (write photon). As a result, an entangled state of the atomic ensemble and the single-photon field is generated. The general scheme of writing and readout is as follows (Fig. 12). We consider atoms with the Λ-type energy level structure. An atomic ensemble containing N atoms is initially prepared in the ground state $|g\rangle$ and then illuminated by a short, coherent, off-resonant pulse of the write field with the wave vector $\mathbf{k}_w$. A combination transition, occurring with a low probability, transfers one of the atoms to the state $|s\rangle$, emitting a photon with the wave vector $\mathbf{k}_{wo}$. Although the write photon is generated with a low probability, its detection unambiguously leads to the conditional preparation of a collective atomic excitation of the form

$$|\phi_s\rangle = \sum_{j=1}^{N} \phi_j \exp\left[i(\mathbf{k}_w - \mathbf{k}_{wo})\mathbf{r}_j\right] |g_1 \ldots s_j \ldots g_N\rangle\,, \qquad (7)$$

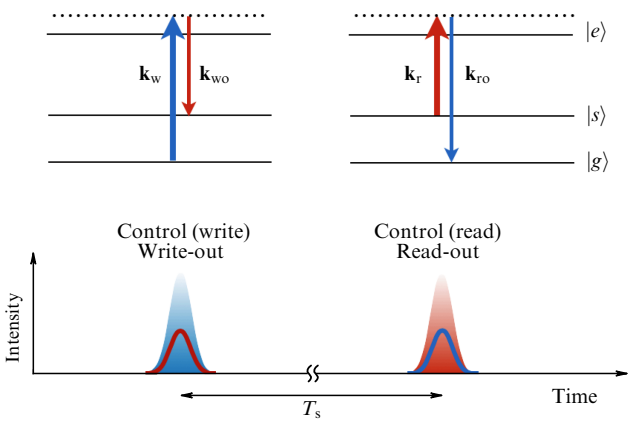

Figure 12. Illustration of operating principle of DLCZ quantum memory (see explanations in text): T_s is information storage time at long-lived transition $|g\rangle \rightarrow |s\rangle$.

which is stored in the quantum memory. This excitation can subsequently be transformed into a readout photon with the wave vector $\mathbf{k}_{ro}$ using spontaneous Raman scattering of a strong readout pulse with the wave vector $\mathbf{k}_r$; as a result, the atomic ensemble will return to its original state. When the phase matching condition is met, the readout photon will be emitted in the $\mathbf{k}_{ro}$ direction with a high probability, which makes the readout process very efficient.

The advantage of the DLCZ method is the maximum efficiency of generating an entangled state of quantum memory and a single-photon field, since the result of spontaneous Raman scattering is equivalent to storing information in an absorption-type quantum memory with unit efficiency. From this point of view, this scheme is ideal for implementing a first-generation quantum repeater, which was demonstrated in [97]. However, to reduce the contribution of multiphoton states to the scattered field, it is necessary to limit the radiation intensity of the write pulse, which significantly reduces the rate of generation of entangled states. In this case, the possibility of DLCZ scheme operation in the multimode regime is limited, in fact, by spatial multiplexing [210–214]. However, a combination of the DLCZ and AFC schemes allows multimode memory to be implemented in the time domain [215], which was demonstrated in doped crystals [216, 217].

3.1.7 Quantum memories with single atoms in cavities. The development of methods for coherently controlling single atoms in cavities makes these systems versatile building blocks for distributing and generating entanglement between nodes of a quantum network. However, their limited mode capacity imposes severe limitations on the rate at which entanglement can propagate in a quantum repeater. Even so, this limitation is mitigated by the potential for deterministic implementation of Bell state measurements [95, 117, 165, 166]. In addition, multiplexing techniques can also be used to increase the rate in the presence of multi-qubit memories, as recently demonstrated in [218–221].

The reversible dynamics of an atomic-field system, which makes it possible to efficiently store and retrieve quantum states of light, can be implemented not only using an ensemble of atoms, but also using a single atom placed in a cavity, in the presence of strong coupling between the atom and the cavity field. Therefore, such a system has long been considered promising for the development of both single-photon sources [222] and quantum network nodes [223–225]. In particular, a Λ-type three-level atom, which strongly interacts with an off-resonant control field at one of the high-frequency transitions and with a cavity mode (also off-resonant) at the other, allows a single-photon state to be highly efficiently generated into a cavity mode with a simultaneous transition of the atom to a long-lived state due to the so-called vacuum stimulated Raman adiabatic passage (v-STIRAP) [114, 226]. From the point of view of quantum communication, such a single-photon source is a single-atom analogue of the DLCZ-based quantum memory, but has an advantage of being deterministic and not making multiphoton contributions to the Raman field. By directing the emitted photons from two such sources to a beam splitter and performing a Bell measurement, it is possible to generate an entangled state between two distant atoms (see Section 2.1.5) [227, 228]. In addition, the emitted photon can be simply transmitted over an optical link and absorbed by another

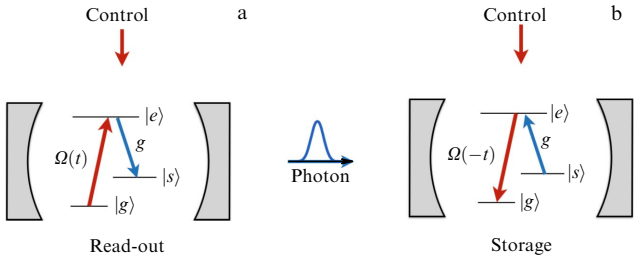

Figure 13. Illustration of operating principle of (left) single-photon source or emitting quantum memory and (right) absorbing quantum memory based on single atoms in a cavity and using stimulated Raman adiabatic transmission (see explanations in text).

atom in the cavity with high efficiency using the stimulated Raman adiabatic passage (STIRAP), which in this case implements the inverse dynamics of the atomic-field system [114, 115, 229]. The basic setup shown in Fig. 13 includes a three-level atom with ground states $|g\rangle$ and $|s\rangle$ and an excited state $|e\rangle$. The optical cavity is coherently coupled to the atom at the $|s\rangle \to |e\rangle$ transition with a coupling constant g, and a classical field with Rabi frequency $\Omega(t)$ controls the atom at the $|g\rangle \to |e\rangle$ transition. If the field is turned on adiabatically, the state $|g, 0\rangle$ is transformed into the state $|s, 1\rangle$, and the state $|s, 0\rangle$ remains unchanged, where $|g, n\rangle$ and $|s, n\rangle$ denote the states in which the atom is in the states $|g\rangle$ and $|s\rangle$, respectively, and the cavity field contains n photons. This process corresponds to the deterministic generation of a single-photon state (Fig. 13a). When the field is turned off adiabatically, the inverse transformation occurs, which is used to store the single-photon state (Fig. 13b). The absence of resonance between the control field and the atomic transition makes it possible to not transfer the population to the excited level and to eliminate losses due to spontaneous emission. Moreover, the presence of resonant transitions with different polarizations in atoms allows one to store and retrieve states encoded in the polarization basis [230], as well as to generate (ideally in a deterministic manner) polarization-entangled states between unheralded single-atom nodes [115].

3.2 Comparative analysis of promising materials for quantum memory

The search for new materials that can keep stored quantum information for a sufficiently long time is a fundamental issue. Many years of experience in developing the hardware for information systems and technologies stipulates the priority of research in the field of solid-state systems. Here, particular emphasis is placed on crystals doped with rare-earth ions [174, 231–233], since they have a number of properties that are very important for storing, processing, and transmitting quantum information:

- long time of maintaining coherence both at optical (several ms) and ultrafine (up to several hours) transitions;
- large ratio of inhomogeneous and homogeneous widths of resonant transitions (up to 10^6), which determines high mode capacity in the frequency-time domain;
- high density of active ions/atoms, making it possible to provide high optical thickness with small sample sizes;
- absence of thermal diffusion, compactness, simplicity, ease of handling, and improved mechanical stability; and
- ability to be connected to other integrated quantum devices, i.e., single-photon sources and detectors.

The most important parameter of quantum information carriers, determining the storage time, is the coherence time. In most systems, decoherence is caused by fluctuations in magnetic fields, in particular, fluctuations in the fields produced by the nuclear spins of crystal atoms in the locations of rare-earth ions. These fluctuations lead to irreversible phase shifts and attenuation of the amplitude of induced dipole moments, which are excited during absorption (storage) of photons and carry the stored quantum information. Consequently, the coherent properties of the medium can be significantly improved, for example, by choosing monoisotopic crystals with minimal concentrations of nuclear spins surrounding impurity ions. The above-mentioned increase in the concentration of rare-earth ions above a certain threshold also leads to a decrease in the coherence time due to the occurrence of interactions between these ions.

At low temperatures, from 1.5 to 4 K, at which such experiments are usually carried out, the coherence times at optical and hyperfine transitions are limited by spin–spin interactions of rare-earth ions with each other and with the atoms of the crystal in which they are located. To reduce these interactions, crystalline matrices with a low density of nuclear spins (for example, Y_2SiO_5) and small (less than 1%) concentrations of rare-earth elements are used. Non-Kramers rare-earth elements, such as praseodymium Pr (with a transition wavelength of $\lambda = 606$ nm), europium Eu ($\lambda = 580$ nm), and thulium Tm ($\lambda = 793$ nm), have suppressed electron spin moments in the ground state, which leads to weak spin–spin interactions. Kramers ions of erbium Er ($\lambda = 1530$ nm) and neodymium Nd ($\lambda = 880$ nm) do not exhibit this suppression, resulting in stronger interactions both between rare earth ions and between ions and lattice atoms, which leads to a decrease in the coherence time. Nevertheless, strong external magnetic fields make it possible to obtain optical coherence times of several milliseconds for erbium-doped crystals with Kramers ions, such as Y_2SiO_5. In neodymium- and praseodymium-doped crystals, the optical coherence times are hundreds of microseconds. It should be noted that the use of dynamic decoupling methods (see reviews [234, 235]) and full clock transitions, which are also called zero first-order Zeeman (ZEFOZ) transitions [236, 237], makes it possible to significantly increase the coherence times of both hyperfine and optical transitions. To date, the longest phase relaxation time for the spin transition of impurity ions has been achieved in the $Y_2SiO_5:Eu^{3+}$ crystal — up to 6 h at temperatures of 1.4 K [238] and 6 K [239] and up to 13 h at a temperature of 125 mK [239] (with the relaxation time of the nonequilibrium population of spin sublevels reaching 23 days [240]). This fact makes this crystal the most promising material for quantum repeaters. It is important to note that an increase in coherence time for both optical and spin transitions upon cooling crystals doped with rare-earth ions to ultra-low temperatures (below 1 K) was demonstrated previously in a number of experiments [241–245]. Thus, it can be asserted that such temperatures are necessary to achieve the maximum possible values of relaxation times. On the other hand, the observation of multi-hour spin coherence times at 6 K is an important step in terms of simplifying the cooling system and placing long-lived quantum memory devices on satellites.

When considering solid-state quantum memory, we should also mention ensembles of nuclear spins in epitaxial quantum dots, since such systems can integrate spin quantum memory and a single-photon source [58]. In quantum dots, storage and retrieval of quantum states of light on a spin subsystem are possible using an electron qubit as an intermediary [246, 247], with the spin coherence time reaching 100 ms (at a temperature of 4.2 K, an external magnetic field of 5.16 T, and the use of dynamic decoupling) [248], which is already sufficient to test the concept of quantum repeaters.

Among other promising materials for quantum memory, we should also mention alkali metal vapors, which demonstrate coherence times of ~ 1 s at room temperature [249]. Moreover, alkali atoms can act as intermediaries for the interaction of the light field with the nuclear spins of noble (inert) gases, the coherence time of which can potentially reach hours [250]. These results are of great interest from the point of view of developing long-lived quantum memory and a quantum repeater operating at room temperature [251, 252]. One of the recent results in this area is the creation of a high-quality entangled state of quantum memory based on ^{87}Rb vapor and a single-photon field at a telecommunication wavelength of 1324 nm [253]. In this case, an ensemble of rubidium atoms was used not only for memory, but also for generating entangled two-photon states (at wavelengths of 1324 nm and 795 nm), so that storage of one of the photons in the memory did not require additional frequency conversion. Also worth noting is a recent experiment on generating entanglement between ^{133}Cs atomic ensembles at room temperature [254].

To date, the record-high values of information storage time in experiments on quantum memory with attenuated laser pulses are ~ 1 s in ^{133}Cs atoms at room temperature [249], ~ 10 s in cold ^{87}Rb atoms [255], and ~ 20 s in cold Cs atoms [256]. Also demonstrated were storage times of ~ 1 min and ~ 1 h in a $Y_2SiO_5:Pr^{3+}$ crystal using the EIT protocol [257] and a $Y_2SiO_5:Eu^{3+}$ crystal using the AFC protocol [258], respectively. When writing optical signals at the single-photon level, the longest storage time (~ 1 s) was achieved in ^{87}Rb atoms [259].

As for multi-qubit quantum memory, two-component (hybrid) systems combining a communication qubit and a memory qubit are very promising. A typical example is color centers in diamond interacting with the ^{13}C nuclear spin or other spins (see review [40]). Notably, Stas et al. [260] have recently demonstrated a quantum network node based on an SiV center in diamond (a communication qubit) interacting with an ^{29}Si nuclear spin (a memory qubit) with a coherence time of more than two seconds at liquid helium temperature. Grimm et al. [261] have reported the results of coherent control of ^{13}C nuclei interacting with one GeV center, which can form the basis of a multi-qubit register. The use of dynamic decoupling methods made it possible to increase the nuclear spin coherence time from 2 ms to 2.5 s at mK temperature. A similar approach can be implemented based on pairs of ions in traps [262, 263], the coherence times of which reach 1 h [264]. Such systems are very promising for quantum repeaters [117, 165, 265].

A very interesting and relevant issue is the combination of the capabilities of multimode atomic-ensemble quantum memory (convenient for multiplexing) and multi-qubit quantum memory (convenient for processing quantum information). Thus, Gu et al. [266] proposed a structure of a quantum repeater that makes it possible, by means of such a combination, to simultaneously obtain multiplexing, deterministic generation of entangled photon pairs, and nearly deterministic entanglement swapping. It is also worth

mentioning the paper by Cussenot et al. [267], who showed that the presence of a cavity allows the AFC protocol to be modified in such a way that a change in the shape of the light pulse makes it possible to connect repeater nodes based on ensembles of rare-earth ions and nodes based on single atoms, which differ greatly in spectral characteristics.

3.3 Review of experimental achievements in field of quantum memory

The efficiency of first-generation quantum repeaters depends markedly on the possibility of long-term storage of quantum states in quantum memory devices and on the prospects for using multiplexing methods. Therefore, much attention is currently being focused on the development of quantum memory devices based on polyatomic ensembles that allow various quantum states of the electromagnetic field, in particular single-photon wave packets, to be stored and retrieved in the multimode regime, thereby implementing high-order multiplexing. Among the most striking experimental results, one can note the demonstration of the high efficiency of quantum memory protocols based on electromagnetically induced transparency (up to 92%) [185, 268, 269], photon echo (up to 87%) [194, 195, 205, 270–274], off-resonant Raman scattering (up to 82%) [275], storage and retrieval of broadband (THz) photons in a diamond crystal in the off-resonant Raman scattering regime [276], a large (up to 5000) ratio of storage time to pulse duration [277, 278], and storage and retrieval of large (about 1000) pulse sequences [279–281]. Let us consider some of the results in more detail.

Cho et al. [273] presented the results of experiments conducted with an ensemble of cold ^{133}Cs atoms in a magneto-optical trap. Use was made of a gradient echo protocol. An efficiency of 87% was achieved at short storage times. Also, using atom–photon coupling enhancement with a ring cavity, an extraction efficiency of $76 \pm 5\%$ was achieved in the DLCZ scheme at a lifetime $(1/e)$ of 0.22 ± 0.01 s on ^{87}Rb atoms in a magneto-optical trap [259]. A memory system based on electromagnetically induced transparency was described in [282], in which a moderate magnetic field is applied to a cloud of cold atoms to remove the Zeeman degeneracy, and thus the states of the polarization qubits are stored as two magnetic field-insensitive spin waves. The measured average polarization state accuracies are 98.6% at a delay of 200 μs and 78.4% after 4.5 ms. The maximum memory time in a cloud of cold atoms (^{87}Rb) achieved to date is ~ 16 s [255].

Memory protocols based on warm atomic vapors are very attractive, since they do not require a good vacuum system or cooling to cryogenic temperatures. Leung et al. [274] reported microsecond storage of single photons with an efficiency of up to $84 \pm 3\%$ in a gradient echo memory system using an ensemble of warm rubidium atoms with a single-photon source based on spontaneous parametric scattering in a cavity. Guo et al. [275] demonstrated memory based on Raman absorption/emission of photons in ^{87}Rb vapor at room temperature. A memory efficiency of more than 82% is achieved for optical pulses with durations from 6 to 20 ns. Tomography of the states at the memory output when coherent input signals of the single-photon level were applied showed that an unconditional accuracy of 98% was reached. Ji et al. [251] reported a record-high storage time of about 1 s in cesium vapor at room temperature. The development of quantum memory devices based on alkali metal vapor at room temperature [251, 283, 284] is of great interest from the point of view of simplifying and lightening the design, which is especially important for space applications. In this regard, the use of hollow-core light cages, which make it possible to implement quantum memory on a chip inside a gas cell, seems very promising [285]. Finally, it should be noted that the first commercial quantum memory device proposed by Qunnect (www.qunnect.inc) is also based on the EIT effect in rubidium vapor. The device operates at room temperature and provides a memory time of 160 μs with an efficiency of 5–10%.

As noted above, memory protocols based on photon echo in rare-earth ion-activated crystals can be incomplete (using two levels) and complete (using three levels). The two-level protocol has a short storage time, while most quantum repeater protocols require long-term, on-demand quantum memory. However, this does not mean that the two-level variant is useless in the field of quantum communications. Sinclair et al. [159] showed that frequency-multiplexed quantum memory with a fixed storage time can be used to perform quantum repeater tasks. The basic idea is to use multiple modes in the frequency domain to ensure a close-to-one probability of successful Bell measurement at an intermediate node. This protocol can significantly accelerate entanglement distribution compared to direct transmission of single photons, and so quantum memory with a given storage time can also be useful for constructing quantum communication channels. In addition, the two-level AFC protocol can be used in applications such as quantum computing due to its low noise figure, which enables high write/readout accuracy. Since the early work on storage and retrieval of the quantum state of light, many experimental studies have been conducted to improve memory efficiency. In particular, a storage efficiency of 69% was achieved with a storage time of 1.3 μs in a Pr^{3+}:Y_2SiO_5 crystal using the gradient echo protocol [194]. The high efficiency of GEM with the simplest forward signal readout is undoubtedly a great advantage of this approach. The data storage efficiency of the AFC protocol can also be improved by using an impedance-matched cavity [198], which was demonstrated in 2013 [270]. Sabooni et al. [270] used the AFC protocol in a cavity with a weakly absorbing Pr^{3+}:Y_2SiO_5 crystal and obtained an efficiency of 56%. The latest result in this area was reported by Duranti et al. [205], who demonstrated an increase in the efficiency up to 62% in the same crystal.

To obtain long storage times using crystals doped with rare earth ions, long-term collective spin excitation is used. The main problem is the signal-to-noise ratio (SNR), since a strong control field is required to convert optical coherence to spin coherence and vice versa. Typically, noise from control fields is suppressed by using spatial and temporal separation of the control field and the signal pulse or a second crystal as a filter. Coherence times in crystals activated by rare-earth ions are limited by stochastic magnetic interactions between the dopant ions and the host matrix. As noted above, there are several ways to increase the spin coherence time using an external magnetic field and dynamic decoupling. The first one relies on the use of hyperfine transitions or states with a zero first-order Zeeman (ZEFOZ) shift [236, 237], when, in a certain external magnetic field, the spin transition becomes insensitive to magnetic field fluctuations (in the first order) induced by the host. Dynamic decoupling is similar to the above-mentioned photon echo method and is realized by acting on the impurity particles with a sequence of radio-frequency pulses [235]. Notably, using these techniques, coherence times of 6 to 13 h were obtained in the

Eu^{3+}:Y_2SiO_5 crystal for transitions between hyperfine sublevels of the ground state [238, 239]. Holzäpfel et al. [286] reported optical storage for 0.53 s and an efficiency of 3.7% in memory using the dynamic decoupling. Ma et al. [258] reported one-hour storage and an efficiency of 0.035% using a combination of dynamic decoupling and ZEFOZ techniques.

The efficiency of spin wave storage has also been improved in recent years. Using an impedance-matched cavity [272], the storage efficiency in the AFC in a two-level version was 53%, and the storage efficiency of spin waves reached 12% in the $^{153}Eu^{3+}$:Y_2SiO_5 crystal. Kutluer et al. [287] demonstrated a 31% efficiency of spin wave storage using a memory based on stopped light in a long-lived spectral hole at the single-photon level. With a bright source, the efficiency reached 39%.

Of course, decoherence control with static magnetic fields and radio-frequency pulse sequences, used to extend the storage time, as well as the use of multi-pass regimes and cavities to increase the efficiency, are also applicable to other protocols, for example, based on electromagnetically induced transparency. Thus, Hain et al. [288] experimentally demonstrated memory for radiation at a level of several photons in a Y_2SiO_5 crystal doped with rare-earth Pr^{3+} ions. Even without decoherence control, the setup allows single photons of microsecond duration to be stored with an efficiency of 42%. Using dynamic decoupling, a memory storage time of up to 10 s was achieved for weak coherent pulses containing about 10 photons with a storage efficiency of several percent. Note, however, that the residual background noise turned out to be approximately an order of magnitude greater than that required for storing and retrieving single-photon pulses with a long (about a second) storage time. Ma et al. [289] implemented an EIT memory with a cavity in a simple heated atomic cell. Due to the cavity and almost perfect matching, a high memory efficiency of up to $67 \pm 1\%$ and a low noise level close to the quantum noise limit (QNL) were simultaneously achieved.

In addition to storing time and frequency qubits, storage of the polarization states of photons is also of interest. Thus, Zhou et al. [290] used two crystals sandwiched between a half-wave plate to store arbitrarily polarized photons. The compact design of the memory reduced the complexity of the setup and improved stability, allowing an accuracy of 99.9%. This is the highest accuracy ever achieved for storing polarization qubits, which makes this method very promising for applications. An ideologically similar method, but using a single crystal and a multi-pass regime, was implemented by Akhmedzhanov et al. [291, 292] to store polarization states. Zhou et al. [293] demonstrated on-demand quantum memory for polarization qubits using a waveguide made of $^{151}Eu^{3+}$:Y_2SiO_5 crystal. Ions occupying site 2 in the crystal provide nearly uniform absorption for arbitrary polarization states when light propagates along the D2 axis. An accuracy of $99.4 \pm 0.6\%$ was achieved when storing and retrieving polarization qubits at a level of 0.32 photons per pulse and a bandwidth of 10 MHz. A recently proposed Stark-modulated atomic frequency comb (SMAFC) protocol has been used [202, 204, 294]. It should be emphasized here that the idea of combining the Stark effect with the standard atomic frequency comb scheme may prove to be very fruitful. Storage of single-photon states with the transfer of optical coherence to the spin subsystem is difficult to implement due to excessive optical noise generated by the emission of ions excited by strong control pulses. This emission can be a consequence of incoherent fluorescence of ions excited off-resonantly. It can also be coherent emission in the form of (i) a free induction decay (FID) signal emitted due to resonant excitation of background ions under the action of the control field or (ii) unwanted echo emission due to off-resonant excitation of the AFC ensemble. The Stark effect allows the ion ensemble to be separated into two electrically different ion classes, which can be coherently controlled by electric field pulses. When an appropriate electric field pulse is applied, the coherent oscillations of the two ion classes are phase-shifted by 180° before the first optical control pulse is applied. As a result, any coherent emission, including photon echo, is suppressed. The echo emission will also remain suppressed after the control pulses are applied until a second electric field pulse is applied. The second electric field pulse returns the stored collective excitation into phase and simultaneously turns off any coherent processes initiated during the time between the two electric field pulses. In particular, the coherent emission of the control pulses that transfer coherence to the spin state is suppressed. In addition, the control of the electric field provides greater flexibility in choosing the timing of the first control pulse without the risk of re-echoing. The second electric pulse can also be independently adjusted to delay the echo emission after the second control pulse, introducing another degree of control into the spin-wave quantum memory scheme.

In recent years, significant effort has been made to develop integrated quantum memory based on waveguides in rare-earth-doped crystals (see review [295] and recent papers [202, 293, 296–298]). For example, Liu et al. [202] reported on-demand storage and retrieval of qubits in an embedded waveguide memory fabricated on the surface of a $^{151}Eu^{3+}$:Y_2SiO_5 crystal using a Stark-modulated atomic frequency comb protocol. A qubit storage accuracy of 99.3% is achieved using coherent pulses at the single-photon level. Quantum memories based on such structures may have additional advantages in terms of ease of use, robustness, and low loss for scalable network applications (see also [299]). Liu et al. [298] have recently demonstrated quantum memory for photonic qubits with a storage time of 1 ms and an efficiency of 12%. In this case, a noiseless quantum memory protocol based on photon echo was used [300], and millisecond storage times were achieved due to multi-pulse dynamic spin decoupling implemented using a coplanar waveguide. Quantum memory devices on a chip based on single color centers in diamond [301] and on atomic chips are promising options in terms of miniaturization and integration [302].

Efficient multimode quantum memory is a critical resource for long-range quantum communication based on quantum repeaters. Variants of temporal [216, 279–281, 303], frequency [159, 304, 305], and spatial [210–214, 306–308] multiplexing, as well as hybrid schemes [309, 310], are being developed. Afzelius et al. [200] showed that the optimal protocol for implementing multimode quantum memory is the one based on an atomic frequency comb. The width of the AFC spectrum allows many time modes to be efficiently stored without the need to increase the optical thickness of the material. Long-term storage and on-demand readout are achieved by using the transfer of optical coherence to spin transitions. It was shown that AFC quantum memory implemented in solids doped with rare-earth metal ions can store hundreds of modes or more with a close-to-one efficiency. Bonarota et al. [280] presented a convincing

demonstration of the storage of 1060 temporal modes in a thulium-doped crystal using an atomic frequency comb. The comb covered a frequency range of 0.93 GHz. Simultaneous storage of 26 qubits, each containing an average of 0.5 photons, with an accuracy of 97% was demonstrated in [159]. The qubits are written in separate spectral modes and alternating temporal modes, and each is read out individually. A compact and hardware-efficient implementation of a quantum repeater node using a single atomic ensemble for multi-cell (3×4) quantum memory in a cold atom ensemble is reported by Li et al. [311]. The lifetime of an individual memory cell is milliseconds after suppression of the magnetic field-induced inhomogeneous broadening and the atomic motion-induced spin wave dephasing. Pu et al. [211] reported the implementation of a multiplexed DLCZ quantum memory with 225 individually accessible memory cells in a macroscopic atomic ensemble. A spectro-temporally multiplexed quantum memory for single photons at 1532 nm using an atomic frequency comb protocol is implemented in a 10-m cryogenically cooled erbium-doped fiber [312]. The multiplexing covers five spectral band channels — each 10 GHz wide — and each of them uses up to 330 temporal modes, which results in the simultaneous storage of 1650 modes at the single-photon level. Unfortunately, the residual absorption caused by the small branching ratio of the Zeeman sublevels and the short optical coherence time resulted in low efficiency (on the order of 1%) and storage time (slightly more than 200 ns). The experimental implementation of multiplexed quantum memory with many individually accessible memory cells and programmable addressing is an important step for its application in quantum information technologies.

Recently, the storage and retrieval of single-photon and entangled multiphoton states encoded in the orbital angular momentum (OAM) basis of light has attracted attention [313]. Nicolas et al. [314] demonstrated quantum memory for OAM qubits using the electromagnetically induced transparency protocol. According to tomographic measurements, the accuracy achieved during readout was more than 92%. Also, using the EIT protocol in a cold atomic ensemble, quantum memory was implemented for single-photon states encoded in three-dimensional space in the orbital angular momentum. The storage accuracy was $85.3 \pm 1.8\%$ [315]. In their recent work, Ye et al. [316] reported the implementation of quantum memory for OAM qutrits, providing a storage time of 400 μs, which is two orders of magnitude greater than that demonstrated in the previous work. Yang et al. [317] have recently demonstrated high (more than 70%) memory efficiency based on EIT in cold ^{87}Rb atoms in the multiplexing regime using four OAM states and four spatial channels.

An active search for and implementation of quantum memory for telecom photons, as well as efficient methods for converting single photons of the visible range into the telecom range, is underway. Thus, Dajczgewand et al. [318] reported the implementation of the ROSE protocol in a solid doped with erbium, compatible with telecommunication devices. The ROSE scheme is a modification of the standard two-pulse photon echo, making it suitable for quantum memory. An efficiency of 40% for a weak laser pulse in the forward direction has been demonstrated using certain orientations of light polarizations, magnetic field, and crystal axes. However, effort is still required to achieve the required signal-to-noise ratio when storing single-photon pulses. Experiments on the implementation of memory for weak coherent states of light of telecom wavelengths (1536 nm) using an erbium-doped crystal activate (Er^{3+}:Y_2SiO_5) are presented in [204]. Quantum memory protocols based on both controlled reversible inhomogeneous broadening and atomic frequency combs have been investigated. The efficiency was on the order of 1% in both cases. However, quantum memory in the 1550-nm fiber optic data transmission range with a storage time greater than 1 μs has not been demonstrated. It should be noted that this material is quite promising for producing efficient broadband quantum memory at telecom wavelengths. In a study of hyperfine spin dynamics in the presence of a strong magnetic field, a coherence time of 1.3 s was observed [319]. Askarani et al. [299] demonstrated storage and re-emission of single photons with a wavelength of 1532 nm in a cryogenically cooled crystalline waveguide made of lithium niobate doped with erbium. In the experiment, use was made of a photon pair source based on spontaneous parametric scattering and a memory protocol based on an atomic frequency comb with a bandwidth of 6 GHz obtained by burning spectral holes in an inhomogeneously broadened absorption line. The actual memory efficiency was on the order of 0.1%.

On the other hand, the need to match the wavelength of the transition used in the crystal with the telecom wavelength can be eliminated by using quantum frequency conversion. At present, the main developments of such converters are focused on the effects of sum or difference frequency generation in quadratic nonlinear media with waveguide structures, since waveguide arrays are relatively easy to use and, in addition, there are examples of a record-high internal efficiency of the process (above 90%). There are a number of papers in which elements of quantum repeater protocols with an integrated frequency conversion system based on crystals with a waveguide structure are implemented. This topic is discussed in more detail in Section 3.5 of this review.

In conclusion, Table 3 presents examples of experiments on the implementation of long-lived quantum memory, in which information is stored at a low-frequency (spin) transition. This type of memory is of interest for quantum repeaters. Note for comparison that the characteristic memory time in the case of an ideal controlled optical delay line based on optical fiber with a loss of 0.17 dB km^{-1} is 125 μs. The dependence of the efficiency on the storage time for such experiments is presented in review [61].

3.4 Comparative analysis of main methods for generating single-photon and entangled two-photon states of light

3.4.1 Single-photon sources. An ideal source of single photons should meet the following criteria:

- a single-photon wave packet (single-photon pulse) is emitted with unit probability (efficiency), which means that the contribution of the vacuum state or multiphoton states to the source radiation field is zero;
- photons are emitted at any given moment in time (i.e., on demand); and
- successively emitted photons are indistinguishable and correspond to a pure single-photon state (transform-limited pulses).

From the point of view of physical implementation, we distinguish three methods of generating single photons. The first involves the use of a single quantum system, an emitter, in which two energy levels can be isolated and used, with a spontaneous transition between the levels leading to the

Table 3. Examples of experiments on implementing long-lived quantum memory in polyatomic ensembles.

Physical system	Memory schemes	Efficiency [1]	Memory time [2]	Probe pulse duration	Literature
$Y_2SiO_5:Eu^{3+}$	AFC	0.00035 0.065 0.037	26 min 129 ms 0.26 s	2 μs 700 ns 7 μs	[258] [320] [286]
$Y_2SiO_5:Pr^{3+}$	EIT	0.0033 0.01	42 s 2 s	10 μs 20 μs	[257] [184]
Cold Cs atoms	EIT	0.9	325 μs	200 ns	[185]
Cold Rb atoms	DLCZ EIT GEM	0.75 0.14 0.75	220 ms 16 s 1 ms	— 82 ns 6.66 μs	[259] [255] [273]
Cs atoms	EIT	0.14	490 ms	5.5 μs	[249]

[1] Efficiency is defined as ratio of output field energy to input field energy at minimum memory time.
[2] Memory time is determined by efficiency decay level $1/e$ from initial one.

emission of a single-photon wave packet. The resulting sources are deterministic, also called on-demand sources, which can be realized in systems such as semiconductor quantum dots [321–325] (see also review [326]), single molecules [327, 328], single atoms [329], single ions [330, 331], and color centers [332–334]. Single Rydberg atoms, which are released from an atomic ensemble due to the Rydberg blockade effect, can also be included in this category [335]. The second method involves the use of nonlinear optical effects, in which a pair of photons is randomly emitted, so that the detection of one photon heralds the appearance of another one. In this case, we are dealing with heralded probabilistic sources. These single photon sources may be based on spontaneous parametric scattering [336, 337], which is increasingly observed using nonlinear waveguides and microcavities [338, 339]. The third method is to use a strongly nonlinear filter based on the photon blockade phenomenon [340, 341]. In this case, an attenuated laser pulse is directed into a medium that transmits only single-photon states and does not transmit multiphoton states. Such a medium can be a cavity containing a single atom that strongly interacts with the cavity field.

In practice, the distinction between deterministic and probabilistic sources is not clear-cut. Deterministic sources can become more probabilistic with increasing extraction losses or decreasing coupling efficiency, and probabilistic sources can become more deterministic through multiplexing [342–344]. In recent years, significant experimental progress has been observed in improving the characteristics of both options. Incidentally, Ding et al. [345] presented a source based on a quantum dot in a microcavity, with a total efficiency (the probability of a photon appearing at the fiber output of the device) of 71% at an average two-photon interference visibility of 98.56%, which characterizes photon indistinguishability. The obtained efficiency for the first time exceeds the value of $2/3$, which corresponds to the threshold condition for scaling linear optical quantum computing [346]. The previous record-high value of 57% with an average two-photon interference visibility of 97.5% and a generation rate of 1 GHz was obtained in 2021 [347]. However, it should be noted that efficiencies of this level are currently only obtained for sources emitting at wavelengths from 780 to 950 nm. In the case of telecom wavelengths of the O- and C-band, the best value of the photon collection efficiency (the probability of a photon appearing on the first lens) is 36% when using a photonic crystal cavity [348] and 23% when using a circular Bragg cavity [349] (see also review [350]) with an overall efficiency of about 1%.

Among the latest results on increasing the determinism of heralded sources, we can note the work on the use of photon-number resolving detectors [351–353]. Theoretically, this approach makes it possible to increase the probability of conditional preparation of single photons to 25% [354], which significantly simplifies a further increase in the determinism due to various multiplexing methods (see reviews [342, 344]). Such detectors can distinguish up to 32 photons with an overall efficiency of 98%, which provides high accuracy in detecting multiphoton states [355]. Moreover, the number of distinguishable photons can also be significantly increased using spatiotemporal multiplexing techniques [356].

In general, the main advantages of sources based on spontaneous parametric down-conversion (SPDC) or spontaneous four-wave mixing (SWM) are the possibility of generating photons in a wide frequency range, of generating pure quantum states (transform-limited pulses) at room temperatures, and of preparing single-photon pulses of various durations and time shapes. The main disadvantages are the random nature of the generation (during the action of the pump field, pairs of photons are generated at random moments in time) and the nonzero contribution of multiphoton states (in addition to pairs of photons, fours, sixes, etc., are generated). To suppress multiphoton contributions, the pump field intensity is set to be low, which makes the process of generating a photon pair inefficient. The solution to the problem seems to consist, as noted above, in using heralded photon-number resolving detectors and subsequent multiplexing of several nonlinear processes.

The main advantages of sources based on single quantum emitters are the ability to generate on-demand photons and the absence of contributions from two- or multiphoton states. The main disadvantages include the low efficiency of radiation output from a point source (especially when it is located in a high-index material); the incoherent nature of single-photon pulses (lack of spectral limitation) due to the large homogeneous broadening of optical transitions at room temperature; and the uniqueness of each individual center in a solid-state matrix (inhomogeneous broadening of optical transitions), which leads to distinguishability of photons emitted by different centers. In addition, it should be noted that the temporal shape of the emitted single-photon pulses

has the form of a decaying exponential with a sharp leading edge, which complicates the synchronization of light pulses when implementing quantum algorithms and reduces the efficiency of storing and retrieving single-photon pulses in quantum memory devices.

3.4.2 Two-photon sources. An entangled photon source is a device that generates the entangled states required for robust quantum communication and most quantum networking applications. An ideal entangled photon source should satisfy the following criteria [357]:

• a two-photon wave packet is emitted with unit probability (efficiency) at any given time (i.e., on demand);

• the contribution of the vacuum state or multiphoton states to the source radiation field is zero; and

• successively emitted photon pairs are indistinguishable and correspond to the standard Bell state.

There are at least two approaches that are often used in practice to implement entangled photon sources. The first is based on nonlinear parametric processes: spontaneous parametric down-conversion and spontaneous four-wave mixing [338, 343, 358, 359]. Despite the fact that entangled photon pairs are generated without heralded signals in this case, and the efficiency of nonlinear conversion is significantly less than unity, probabilistic generation of entangled pairs using SPDC or SFWM remains a widely used method, mainly due to its relative simplicity and versatility. Photons can be entangled in polarization, frequency, and time, demonstrating a high degree of entanglement. Thus, Zhong et al. [360] have recently reported polarization entanglement using narrow-band spectral filters that eliminate spectral correlations, and have demonstrated high indistinguishability (96%) and heralded efficiency (97%) of single-photon states, which made it possible to prepare 12-photon entangled states.

Typical spectral widths of biphoton fields generated in nonlinear crystals or waveguides are several nanometers, which corresponds to terahertz in the frequency domain. However, storage and retrieval of single photons in quantum memory devices requires a spectral width of about 10–100 MHz, for example, if we are talking about quantum memory based on impurity crystals doped with rare-earth ions. In this regard, the use of SPDC or SFWM in a cavity is promising, which allows the generation spectrum to be narrowed to tens of MHz or less with a simultaneous increase in the spectral brightness of the source [361]. Recently, much attention has been focused on photon pair sources based on SPDC in quadratically nonlinear ring microcavities, which makes it possible to obtain very high efficiency [362] and tune the generation frequency using electric fields.

Small linewidths in a cavity are achieved due to the greater length of the cavity and/or high finesse of the cavity. In particular, a number of studies [363–366] have demonstrated photon sources with a spectral width of less than 1 MHz. Schemes with short cavities and high finesse [367–370] are convenient in that they provide a larger value of the dispersion region (free spectral zone), thereby facilitating and increasing the efficiency of passive filtering, which is usually necessary to isolate one cavity mode at the source output. For example, Monteiro et al. [368] obtained a dispersion region of almost 30 GHz at a small effective cavity length of about 1 cm, which agrees with the multiplexing systems used in optical communications. In this regard, studies of the possibility of single-mode generation of a narrow-band counter-directional SPDC in materials with a short period of nonlinearity modulation [371–376] are of interest, since losses can be avoided when passing through additional filters. In addition, when using a dual-cavity setup, when the cavity maintains both the signal and idle fields, generation in one mode is possible due to the cluster effect [377]. This arrangement has been recently used in [378] to obtain polarization-entangled two-photon states with a spectral width of 500 MHz.

One of the advantages of two-photon sources based on SPDC or SFWM is the possibility of generating correlated photons with very different wavelengths, one of which may correspond to the absorption line in a quantum memory device, and the other may correspond to a fiber-optic communication channel. In this case, the presence of a cavity allows narrow-band photons to be efficiently generated, which can be used to form correlated states of a single-photon field and quantum memory without frequency conversion [379–381]. In addition, narrow-band entangled states can be generated in this regime. Thus, Turaykhanov et al. [382] have recently implemented a source of polarization-entangled photons, one of which is compatible with quantum memory based on a $Y_2SiO_5:Eu^{3+}$ crystal (wavelength 580 nm, spectral width 8 MHz), and the second of which corresponds to the O-band of fiber-optic communication (wavelength 1342 nm). In this case, use was made of a simple compact configuration of a sequence of two periodically poled lithium niobate crystals with crossed optical axes in one common cavity.

Recently, much attention has been paid to the development of methods for generating multifrequency entangled states of a light field, in particular, using a biphoton frequency comb (see review [383]). This approach turns out to be very promising for generating multidimensional quantum states [384–388], including cluster states [389, 390], as well as for high-order frequency multiplexing [386, 391]. The use of frequency encoding is of great interest both for the implementation of a frequency-multiplexed quantum repeater [159, 305, 392] and for quantum information processing in general [383, 393, 394]. In the case of biphoton sources based on SPDC, frequency multiplexing makes it possible to significantly increase the generation rate of entangled qubit pairs (see paper [395] and references therein). In this case, it is possible to generate single-photon qubits in the frequency representation by controlling their state with the pump field [396], thereby minimizing the losses at the source output.

An alternative approach to developing entangled photon sources is the use of emitting cascades in single quantum systems, such as quantum dots [397, 398] (see also review [399]). Thus, Wang et al. [400] reported an entangled photon source based on an InGaAs quantum dot in a circular Bragg cavity, which provides high fidelity (quality) of entanglement (90%), extraction efficiency of photons from the cavity (79%), and photon indistinguishability (90%). Rota et al. [401] reported a 96% fidelity of entangled states with a 69% extraction efficiency (the efficiency at the first lens was 13%) by placing a GaAs/AlGaAs quantum dot in a circular Bragg cavity and controlling the fine structure of the source levels through a piezoelectric actuator. The highest value of the efficiency of photon extraction from a ring Bragg cavity, equal to 85%, with photon indistinguishability of 90% was demonstrated in [402] (while the source efficiency at the first lens was 65%).

3.5 Quantum frequency converters

One pressing problem in the field of quantum network development is frequency conversion of quantum states of light [403]. More specifically, this conversion is necessary to match sources, quantum channels, and memory devices that differ in frequency in order to achieve a maximum efficiency of quantum state distributions. Of particular importance are converters between the optical and microwave ranges [404, 405]. On the one hand, superconducting quantum computers that manipulate quantum information via microwave signals are one of the most advanced platforms for quantum computing. On the other hand, it is generally accepted that optical photons should be used as information carriers for long-distance communication. As a result, a scalable quantum network connecting disparate quantum computers requires a quantum converter that reliably converts quantum signals between microwave and optical regimes (used in quantum computing and quantum communication, respectively). In particular, by combining the deterministic generation of multi-qubit cluster states in superconducting quantum circuits [406] with frequency conversion, it is possible efficiently generate such states in the optical range, which is important for the development of one-way quantum repeaters (see Section 2.2). However, since the difference in energy (frequency) between these two regions exceeds five orders of magnitude, such conversion of microwave radiation into optical radiation turns out to be an incredibly challenging task. To date, the highest conversion efficiency between the microwave and optical ranges has been achieved in optomechanical systems (a membrane in a cavity at a temperature of 0.035 K) and is 47% [407] (see review [408]), which means that the 50% threshold necessary for quantum information processing has yet to be overcome. A significant drawback of such systems is the small conversion bandwidth (in this experiment, 12 kHz).

However, quantum frequency conversion between different optical ranges is also of great practical importance. Such quantum frequency converters (QFCs) are actively used in the development of single-photon detectors [409–411]; interfaces between quantum memory devices and fiber-optic networks, in particular, entanglement of remote quantum memory devices [412–420]; and devices that erase photon color information [421, 422] (see also review [423]). The quality of an ideal quantum converter can be assessed by its high conversion efficiency, wide bandwidth, and low added noise [424]. In addition, a fundamental characteristic is the quantum bandwidth [425], which tends to infinity at unit conversion efficiency and vanishes at a 50% loss (100% in the presence of two-way classical communication) of the signal. To date, frequency conversion based on three- or four-wave mixing has been demonstrated using various platforms, such as nonlinear waveguides [426, 427], nonlinear crystals in cavities [428, 429], microcavities [430, 431], and atomic or molecular systems [432, 433].

Currently, the best results have been demonstrated by sum- or difference-frequency-based QFCs in quadratic-nonlinear media with waveguide structures, since waveguide circuits are relatively easy to use and, in addition, there are examples of work with record-breaking internal efficiency of the process. When using nonlinear waveguides, the internal conversion efficiency can reach 96%, and the resulting efficiency of the device, taking into account all losses, can reach 57% in a single-pass circuit [416, 418]. In this case, the phase-matching conditions for the processes of sum or difference frequency generation make it possible to obtain photons at the output that have a narrow spectrum (several MHz or less). Moreover, when using a waveguide structure, spatial matching of radiation incident on a nonlinear medium is simplified, and the efficiency of interaction of three modes of optical radiation is significantly increased.

If a nonlinear crystal placed in a cavity is used as the main conversion element, the conversion efficiency can reach 80% [428]. This makes it possible to convert states corresponding to high-order transverse modes or spatial images [434]. In addition, such systems can demonstrate a lower noise level compared to that in nonlinear waveguides due to a higher-quality periodic domain structure, which will be discussed below. However, to use this QFC, it is necessary to take into account the intracavity matching conditions, which can lead to a broadening of the output signal to several ten MHz and even to several hundred MHz in the case of a cavity with low finesse. If this type of QFC is to operate together with quantum memory devices, the absorption line width of which is on the order of several MHz, then the useful signal may be lost, which will lead to a general decrease in the quality of the entire system. Moreover, to achieve high frequency conversion efficiency, a high accuracy of spatial matching of the modes interacting inside the cavity is required.

When using integrated optical systems with microcavities, the overall efficiency of the devices can reach 60% [430] at a pump power of less than 60 mW. Since typical materials for microcavities are silicon oxide and silicon nitride, which have cubic nonlinearity, the QFC in these systems is based on Bragg-scattering SFWM. The main advantage of using microcavities is a significant increase in the efficiency of nonlinear processes and, as a consequence, a decrease in the required pump power, which is hundreds of mW in nonlinear waveguides.

In addition to efficiency, a fundamentally important characteristic of the QFC is the noise level. Efficient and low-noise QFCs are usually demonstrated using difference and sum frequency generation (DFG and SFG) for frequency down-conversion (frequency up-conversion) in materials with quadratic nonlinearity. Notably, low noise is possible in situations where the required spectral shift is small enough that the pump field is well separated from the input signal and the frequency-converted idler and has the longest wavelength. This configuration provides low noise in platforms such as lithium niobate waveguides with a periodically poled structure and has been used in a number of experiments, for example, to convert single photons with a wavelength of 900–950 nm emitted by quantum dots to photons with a telecom wavelength of 1550–1560 nm [435, 436]. However, for quantum memory operating at shorter wavelengths, differing from the C-band by more than a factor of two, it is no longer possible to use the pump as the field with the longest wavelength (within a single-step conversion process). As a result, the presence of a strong pump field in the range between the input signal and output idler fields leads to the appearance of noise caused by Raman scattering, fluorescence, and parasitic SPDC (Fig. 14a).

The currently known approaches to solving the problem are spectral filtering (usually accompanied by large insertion losses), down-conversion to 1310 nm [437], and a two-stage conversion process in which long-wavelength pumping is used at each stage [438]. The contribution of parasitic SPDC caused by imperfections in the periodically poled structure [439] can be reduced by better fabrication of the nonlinear

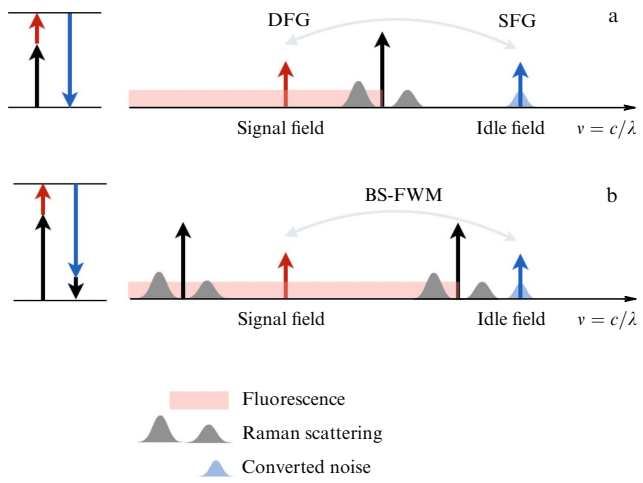

Figure 14. Illustration of noise sources in process of quantum frequency conversion based on (a) sum (difference) frequency generation in quadratic nonlinear materials and (b) Bragg-scattering four-wave mixing (BS-FWM).

crystal, which was recently demonstrated using the example of a QFC of photons emitted by NV centers [429]. In the case of a QFC based on four-wave mixing with Bragg scattering, the frequency shift is determined by the difference between the frequencies of the two pump fields, and when large frequency shifts are required, the same problem arises, since the frequency of one of the pump fields is located between the frequencies of the signal and idler fields (Fig. 14b). One promising option for solving the problem is to use sum (difference) frequency generation in materials with cubic nonlinearity [440], in which the pump field can have a long wavelength even in the case of a short-wavelength signal field.

In conclusion, we note that, from the point of view of frequency multiplexing in quantum repeaters or single-photon sources, an important task is to implement, not frequency conversion, but a small frequency shift (frequency shifting) of quantum states in order to achieve their indistinguishability. This problem can be solved using phase light modulators acting directly on the signal field [441–444] or on the pump field used in the QFC [445, 446].

4. Review of experimental achievements towards implementation of an elementary segment of a quantum repeater

Currently, a number of experiments have been performed to generate entangled states of two quantum memory devices, representing both individual atoms (qubits) and atomic ensembles. The most widely used method for generating heralded entanglement is based on Bell measurements, which have been demonstrated using ^{87}Rb atoms [228, 418, 447], $^{171}Yb^{+}$ ions [227, 448], $^{88}Sr^{+}$ ions [449], $^{40}Ca^{+}$ ions [450], $^{138}Ba^{3+}$ ions [451], NV centers in diamond [452–455], SiV centers in diamond [43], InGaAs quantum dots [456, 457], single $^{171}Yb^{3+}$ impurity ions in YVO_4 crystals [220], ensembles of cold ^{87}Rb atoms [42, 415, 458–460], vapors of ^{133}Cs atoms [254, 461], and impurity crystals of Pr^{3+}:Y_2SiO_5 [462] and Nd^{3+}:YVO_4 [463]. The most important parameters characterizing progress in this area are the distance between the devices (the quantum channel length), the probability of generation per attempt, and the rate of generation of the entangled state. In addition, an important parameter is the ratio of the last to the decay rate of the quantum memory, since the larger this value, the greater the possibility of using the generated entanglement in long-range quantum communication. This ratio is sometimes called the link efficiency [225]. In particular, with an efficiency higher than $\cong 0.83$, a deterministic distribution of entanglement becomes possible [454]. To date, a link efficiency greater than unity has only been achieved at short distances (about 1 m) [448, 454], which indicates the difficulty of demonstrating scalable quantum communication based on quantum repeaters. In this case, the values of the probability of generation per attempt reach an order of 10^{-4} [454, 456, 457], and the generation rate can reach kHz [254, 456, 457, 462]. However, at distances of 30–50 km, the generation rates drop significantly: 1/85 s^{-1} [418] and 1/0.65 s^{-1} [460]. Note that much higher values of the probability of generation per attempt can be obtained using other schemes, such as forwarding and absorption (2×10^{-2}) [115] and distributed logical operation (6×10^{-3}) [107]. The use of quantum memory with multiplexing also makes it possible to significantly increase the link efficiency [213, 303]. Thus, Zhang et al. [213] demonstrated an entanglement generation efficiency of 0.46 through a 12-km-long fiber optic channel due to the multiplexing of 70 spatial and four angular modes.

Among the latest experiments, we can mention the generation of entangled states between quantum memory devices connected to each other via urban fiber-optic communication channels about 10 km in length [41–43]. Liu et al. [42] constructed a network of three nodes containing quantum memory based on cold ^{87}Rb atoms which were entangled with single-photon states using the DLCZ scheme and one server allowing any two nodes to be entangled via a single-photon Bell measurement. The probability of conditional entanglement preparation reached 8×10^{-4}. Single-photon frequency converters with a total efficiency of 46% were used. Stolk et al. [41] prepared entanglement between two nodes based on single NV centers in diamond using a protocol that assumed a single-photon Bell measurement at an intermediate station. Each node was equipped with a single-photon frequency converter with an efficiency of about 50%, and the probability of successful entanglement generation per attempt in the post-selection mode (the states of the qubits are measured before the Bell measurement and then selected taking into account the result of the latter) was 7.2×10^{-6}. Finally, Knaut et al. [43] were the first to implement quantum communication between two nodes based on SiV centers in a nanophotonic diamond cavity, where spin states of ^{29}Si, demonstrating coherence times of about 2 s [260], were used for information storage. In this case, an entanglement generation protocol was used based on the sequential interaction of a single-photon pulse with two qubits, followed by measurement of the single-photon state [464] (see Section 2.1). The success probability was 2×10^{-5} and was limited mainly by the efficiency of single-photon frequency conversion (5.4%).

In addition, particular mention should be made of the first implementation of quantum communication between two single rare-earth ions in impurity crystals [220]. The authors of this paper succeeded not only in generating an entangled state of two ytterbium ions in different YVO_4 crystals made in the form of nanophotonic cavities, but also in preparing a three-qubit entangled W-state using two ions in one crystal. Moreover, they proposed a method for compensating for the

frequency fluctuations of the optical transitions of ions, which opens up the possibility of scaling the technique using frequency multiplexing. The capabilities of such multiplexing were demonstrated using two ions at each node, which made it possible to increase almost twofold the rate of entanglement generation between nodes.

In addition to experiments on entangling two quantum memory devices, problems of memory-assisted quantum key distribution, aimed at implementing hardware-independent quantum cryptography protocols by replacing trusted nodes with untrusted ones, are also being solved. Among the latest experiments in this field, we can mention the implementation of hardware-independent quantum key distribution (QKD) via optical fiber using quantum memory based on cold ^{87}Rb atoms [465] and $^{88}Sr^{+}$ ions in traps [466], with the vulnerability of detection due to violation of Bell's inequality being eliminated. On the other hand, Yin et al. [467] experimentally implemented the E91 QKD protocol using an untrusted satellite node and demonstrated the distribution of entangled photons over a record-high distance of 1200 km. Further progress in the deployment of multi-node hardware-independent networks requires the practical implementation of efficient quantum repeaters. Among the studies in this area, we can note paper [468], which demonstrated that the use of a single intermediate node increases the rate of the measurement-device-independent QKD (MDI-QKD) compared to direct transmission. In this work, it was possible to demonstrate an improvement in the rate relative to the PLOB bound [69] and a fourfold increase in the QKD rate compared to the experiment where direct transmission was used [469]. In this case, the intermediate node consisted of a single SiV center built into a photonic crystal cavity, which had a coherence time of 0.2 ms at a temperature of 300 mK. In the future, a single SiV center can use several of its ^{13}C neighbors to design a multi-qubit register [464] and implement deterministic Bell measurement or error correction.

The next experiment in this sphere was a demonstration of QKD using an intermediate node containing two ^{87}Rb atoms in the cavity [470]. Both atoms were entangled with photons that were sent to two users via optical fibers, and the resulting photon entanglement was achieved by swapping due to a Bell measurement with two atoms. The resulting QKD rate was as high as 0.57 bit s^{-1}, which corresponded, as expected, to a twofold increase in the velocity decay length as a function of distance.

Finally, among the most recent experiments, one can note the paper by Krutyanskiy et al. [419], who used an intermediate node with two $^{40}Ca^{+}$ ions in the cavity. The resulting entanglement distribution rate was 9.2 Hz with a total fiber line length of 50 km between the end points. In this case, the quality of the distributed entangled state was 0.7. Using two ions in one node is also a promising approach for implementing a deterministic Bell measurement.

Finally, let us dwell on the issues of constructing multi-node quantum networks. Due to the technical complexity of the problem, an obvious direction for development is to build small networks in a laboratory setting and then scale them up. Recent paper [471] presents the first implementation of such a small quantum network consisting of three nodes, each containing quantum memory for local processing of quantum information. The nodes were linked by optical fibers about 10 m in length, and the quantum memory was the electron spin of an NV center in diamond, which played the role of a qubit for communication. Additionally, one of the nodes used a nuclear spin of ^{13}C that is close to the color center, which played the role of a qubit for memory. Several multi-node operations were performed using this network, such as the generation of a three-qubit Greenberger–Horne–Zeilinger state and entanglement swapping. In particular, after generating heralded entanglement between the NV center at Alice's node and the NV center at Charlie's node, Charlie's electron spin state was transferred to the ^{13}C nuclear spin, so that the electron spin of the NV center could be used again to generate entanglement with a third NV center at Bob's node. This left two qubits at one node (Charlie), with which a Bell measurement could be made and entanglement implemented between Alice's and Bob's qubits. This experiment was the first demonstration of entanglement swapping between remote nodes that were not initially connected to each other. The resulting Bell state generation rate between Alice's and Bob's spin qubits was 25 MHz and the fidelity was 55%. In a subsequent experiment [472], this network was also used to teleport quantum information between two remote nodes. Such networks can obviously be viewed as a testing ground for real-world applications and testing of various quantum communication protocols.

5. Quantum repeaters and space communications

Quantum communication with satellites has long been considered a promising technology for distributing entanglement over long distances [473–477]. There has been significant experimental progress in this regard [478–483]. Since photon losses in space are much smaller than those in the atmosphere or optical fiber, increasing the distance of quantum communication using a satellite quantum network seems quite promising. This is also facilitated by the movement of satellites in orbit. The main difficulty arises at the stage of photon reception, when the aperture of the receiving telescope is significantly smaller than the diameter of the beam that has traveled a long distance or traveled through a turbulent atmosphere. In addition, the movement of satellites around Earth requires a high-precision guidance system and limits the time of quantum communication. In this regard, the use of medium-altitude or geostationary satellites seems promising. In terms of practical application, an obvious disadvantage of quantum communication between space and ground stations is the strong dependence on weather conditions and time of day. Detailed simulation of the efficiency of space quantum communication taking into account various factors is given in a number of papers [474, 484–487].

An urgent avenue of research is the development of hybrid quantum repeater schemes that combine the advantages of space communication and quantum memory. For instance, in order to extend the range of operation of the simplest first-generation quantum repeaters, Boone et al. [488] proposed a scheme in which the sources of entangled photon pairs are located aboard orbital satellites, and the memory is at ground stations. It was shown that practically significant quantum key distribution rates can be obtained for intercontinental distances, even with a small number of ground stations. However, good weather conditions should be assured for each ground station during the operation of the entire communication line, which is extremely unlikely. A completely space-based quantum repeater system was proposed and analyzed in [486, 489]. It is expected that launching all components in space will accelerate the intercontinental

entanglement distribution rate by several orders of magnitude for a first-generation quantum repeater. Wallnofer et al. [490] used Monte Carlo simulation to demonstrate that an intercontinental quantum key distribution rate in the kHz range is reasonably attainable with three satellites, one of which carries two quantum memory cells. The characteristics of the memory devices used, in particular, a high mode capacity and a memory time on the order of 100 ms, seem achievable in the medium term. Finally, Gündoğan et al. [491] considered the option of using only one satellite with two quantum memory devices, a source of entangled photons, and a Bell measurement unit as a mobile quantum memory node. This option is simpler than the one with a constellation of satellites, but it is necessary that one of the memory devices be not only multimode (the degree of multiplexing is on the order of 10^5), but also ultra-long-lived (memory time on the order of 1 h).

From the point of view of placing quantum memory on satellites, the development of compact devices on the same physical platforms that are used for on-board atomic clocks seems promising. Of interest are memory cells based on alkali metal vapors functioning at room temperature, as well as on the basis of impurity crystals, demonstrating multi-hour coherence times at temperatures above 4 K (see Section 3.2).

6. Conclusions

The development of quantum repeaters is one of the urgent and fundamental tasks in the field of quantum technology. The possibility of implementing an efficient first-generation quantum repeater significantly depends on successes in the field of designing long-lived quantum memory, and so, in the near future, the main effort will be aimed at combining a long storage time, high efficiency, and high mode capacity in one device. However, in terms of future practical application, it should be noted that current versions of long-lived quantum memory imply the use of impurity crystals at the temperature of liquid helium or cold atoms. Perhaps such devices are suitable for constructing an extended terrestrial network, but it is difficult to imagine that such intermediate nodes will be installed on intercontinental trunk communication lines laid on the ocean floor. Therefore, particularly relevant areas of research are (i) the creation of solid-state quantum memory capable of functioning at temperatures higher than that of liquid helium (the recent observation of multi-hour spin coherence times in $Y_2SiO_5{:}Eu^{3+}$ crystal at 6 K opens up the possibility of demonstrating such quantum memory); (ii) the creation of quantum memory capable of functioning at room temperature (in this regard, quantum memory based on a gas mixture of alkali metal and inert atoms is of great interest); and (iii) the development of hybrid quantum repeater circuits that combine the advantages of space communication channels and quantum memory. The use of a constellation of satellites with quantum memory aboard will not only scale the quantum network, but also ensure an almost continuous distribution of entangled states between ground stations.

In addition, the most important task is still the development of deterministic sources of single-photon or two-photon states of light, which can be used, among other things, to implement a one-way quantum repeater based on cluster states. In the near future, we can expect further improvement of deterministic sources based on quantum dots in terms of increasing the overall efficiency. Moreover, of promise is an increase in the determinism of heralded sources by using photon-number resolving and multiplexing detectors.

In terms of designing mutually coordinated systems of sources, memory, and fiber-optic communication lines, of importance is the development of methods for frequency conversion of quantum states of light. A quite high efficiency of quantum frequency converters has already been demonstrated in experiments, but there are still problems related to the reduction in the noise level in applications where the frequency shift is greater than an octave, which is what is needed in many cases. In addition, to connect superconducting processors into a single quantum network, converters of quantum states of light between the microwave and optical ranges are needed, the development of which is also of great interest. In fact, the emergence of the need to combine many quantum computers seems to be one of the main drivers for the development of full-fledged quantum networks (scaling of QKD networks has so far been successfully achieved through trusted nodes). Finally, an interesting area is the development of methods for frequency conversion between the terahertz and optical ranges, the implementation of which can become the basis for the development of terahertz quantum optics.

Another topical area of research in the near future is the development of deterministic optical Bell measurement schemes, which is equivalent to the development of deterministic optical CNOT gates. Such gates will improve the efficiency of not only various quantum repeaters, but also multi-user quantum communication protocols based on multiphoton entangled states. Since methods for implementing deterministic Bell measurements using pairs of atoms or ions have already been proposed, while quantum memory based on atomic ensembles already demonstrates great multiplexing capabilities, a promising area of research is the development of schemes for transferring information between atomic ensembles and individual memory qubits. This approach corresponds to the known logic of development towards hybrid systems, combining a multi-atom ensemble as a multi-mode interface and individual qubits as quantum registers.

References

1. Vazirani U, Vidick T *Phys. Rev. Lett.* **113** 140501 (2014)
2. Zapatero V et al. *npj Quantum Inf.* **9** 10 (2023)
3. Cirac J I et al. *Phys. Rev. A* **59** 4249 (1999)
4. Monroe C et al. *Phys. Rev. A* **89** 022317 (2014)
5. Cuomo D, Caleffi M, Cacciapuoti A S *IET Quantum Commun.* **1** (1) 3 (2020)
6. Caleffi M et al. *Computer Networks* **254** 110672 (2024)
7. Liu X et al. *Nat. Commun.* **15** 8529 (2024)
8. Main D et al. *Nature* **638** 383 (2025)
9. Barral D et al. *Comput. Sci. Rev.* **57** 100747 (2025)
10. Broadbent A, Fitzsimons J, Kashefi E, in *Proc. of the 50th Annual IEEE Symp. on Foundations of Computer Science, FOCS 2009, 25–27 October 2009, Atlanta, GA, USA* (Piscataway, NJ: IEEE, 2010) p. 517, https://doi.org/10.1109/FOCS.2009.36
11. Barz S et al. *Science* **335** 303 (2012)
12. Fitzsimons J F *npj Quantum Inf.* **3** 23 (2017)
13. Wei Y-C et al. *Science* **388** 509 (2025)
14. Jozsa R et al. *Phys. Rev. Lett.* **85** 2010 (2000)
15. Giovannetti V, Lloyd S, Maccone L *Nature* **412** 417 (2001)
16. Kómár P et al. *Nat. Phys.* **10** 582 (2014)
17. Ilo-Okeke E O et al. *npj Quantum Inf.* **4** 40 (2018)
18. Zhao S-R et al. *Phys. Rev. X* **11** 031009 (2021) https://doi.org/10.1103/PhysRevX.11.031009
19. Beloy K et al. (Boulder Atomic Clock Optical Network (BACON) Collab.) *Nature* **591** 564 (2021)

20. Nichol B C et al. *Nature* **609** 689 (2022)
21. Giovannetti V, Lloyd S, Maccone L *Phys. Rev. Lett.* **96** 010401 (2006)
22. Degen C L, Reinhard F, Cappellaro P *Rev. Mod. Phys.* **89** 035002 (2017)
23. Ge W et al. *Phys. Rev. Lett.* **121** 043604 (2018)
24. Zhuang Q, Zhang Z, Shapiro J H *Phys. Rev. A* **97** 032329 (2018)
25. Pirandola S et al. *Nat. Photon.* **12** 724 (2018)
26. Guo X et al. *Nat. Phys.* **16** 281 (2020)
27. Zhang Z, Zhuang Q *Quantum Sci. Technol.* **6** 043001 (2021)
28. Bothwell T et al. *Nature* **602** 420 (2022)
29. Liu L-Z et al. *Nat. Photon.* **15** 137 (2021)
30. Malia B K et al. *Nature* **612** 661 (2022)
31. Kim D-H et al. *Nat. Commun.* **15** 266 (2024)
32. Bate J et al., arXiv:2501.08940
33. Gottesman D, Jennewein T, Croke S *Phys. Rev. Lett.* **109** 070503 (2012)
34. Khabiboulline E T et al. *Phys. Rev. Lett.* **123** 070504 (2019)
35. Kaltenbaek R et al. *Exp. Astron.* **51** 1677 (2021)
36. Kimble H J *Nature* **453** 1023 (2008)
37. Wehner S, Elkouss D, Hanson R *Science* **362** eaam9288 (2018)
38. Sukachev D D *Phys. Usp.* **64** 1021 (2021); *Usp. Fiz. Nauk* **191** 1077 (2021)
39. Fang K et al. *Sci. China Inf. Sci.* **66** 180509 (2023)
40. Ruf M et al. *J. Appl. Phys.* **130** 070901 (2021)
41. Stolk A J et al. *Sci. Adv.* **10** eadp6442 (2024)
42. Liu J-L et al. *Nature* **629** 579 (2024)
43. Knaut C M et al. *Nature* **629** 573 (2024)
44. Pirker A, Dür W *New J. Phys.* **21** 033003 (2019)
45. Van Meter R et al., in *2022 IEEE Intern. Conf. on Quantum Computing and Engineering, QCE, 18–23 September 2022, Broomfield, CO, USA* (Piscataway, NJ: IEEE, 2022) p. 341, https://doi.org/10.1109/QCE53715.2022.00055; arXiv:2112.07092
46. Shapourian H et al., arXiv:2501.05598
47. Bel O, Kiran M *Computer Networks* **263** 111204 (2025)
48. Ma X-S et al. *Nature* **489** 269 (2012)
49. Takesue H et al. *Optica* **2** 832 (2015)
50. Wootters W K, Zurek W H *Nature* **299** 802 (1982)
51. Salvail L et al. *J. Comput. Security* **18** (1) 61 (2010)
52. Chen Y-A et al. *Nature* **589** 214 (2021)
53. Briegel H-J et al. *Phys. Rev. Lett.* **81** 5932 (1998)
54. Dür W et al. *Phys. Rev. A* **59** 169 (1999)
55. Sangouard N et al. *Rev. Mod. Phys.* **83** 33 (2011)
56. Munro W J et al. *IEEE J. Select. Top. Quantum Electron.* **21** (3) 78 (2015)
57. Yan P-S et al. *Europhys. Lett.* **136** 14001 (2021)
58. Neuwirth J et al. *Mater. Quantum Technol.* **1** 043001 (2021)
59. Wei S-H et al. *Laser Photon. Rev.* **16** 2100219 (2022)
60. Azuma K et al. *Rev. Mod. Phys.* **95** 045006 (2023)
61. Kalachev A A *Bull. Lebedev Phys. Inst.* **50** (Suppl. 12) S1312 (2023); Translated from Russian: *Kvantovaya Elektron.* **53** 609 (2023)
62. Tittel W et al. *Quantum Sci. Technol.* **10** 033002 (2025); arXiv:2501.06110
63. Żukowski M et al. *Phys. Rev. Lett.* **71** 4287 (1993)
64. Bennett C H et al. *Phys. Rev. Lett.* **76** 722 (1996)
65. Deutsch D et al. *Phys. Rev. Lett.* **77** 2818 (1996)
66. Shor P W *Phys. Rev. A* **52** R2493 (1995)
67. Knill E, Laflamme R *Phys. Rev. A* **55** 900 (1997)
68. Pirandola S *Commun. Phys.* **2** 51 (2019)
69. Pirandola S et al. *Nat. Commun.* **8** 15043 (2017)
70. Bennett C H et al. *Phys. Rev. Lett.* **70** 1895 (1993)
71. Gottesman D, Chuang I L *Nature* **402** 390 (1999)
72. Hacker B et al. *Nature* **536** 193 (2016)
73. Tiarks D et al. *Nat. Phys.* **15** 124 (2019)
74. Stolz T et al. *Phys. Rev. X* **12** 021035 (2022) https://doi.org/10.1103/PhysRevX.12.021035
75. Calsamiglia J, Lütkenhaus N *Appl. Phys. B* **72** 67 (2001)
76. Lee S-W, Ralph T C, Jeong H *Phys. Rev. A* **100** 052303 (2019)
77. Yan P-S et al. *Sci. China Phys. Mech. Astron.* **66** 250301 (2023)
78. Werner R F *Phys. Rev. A* **40** 4277 (1989)
79. Devitt S J, Munro W J, Nemoto K *Rep. Prog. Phys.* **76** 076001 (2013)
80. Cai W et al. *Fundamental Res.* **1** (1) 50 (2021)
81. Chatterjee A, Phalak K, Ghosh S, in *2023 IEEE Intern. Conf. on Quantum Computing and Engineering, QCE, 17–22 September 2023, Bellevue, WA, USA* (Piscataway, NJ: IEEE, 2023) p. 70, https://doi.org/10.1109/QCE57702.2023.00017; arXiv:2304.08678
82. Preskill J *Quantum* **2** 79 (2018)
83. Lau J W Z et al. *AAPPS Bull.* **32** 27 (2022)
84. Siddardha Chelluri S et al., arXiv:2503.21569
85. Azuma K, Tamaki K, Lo H-K *Nat. Commun.* **6** 6787 (2015)
86. Zwerger M, Briegel H J, Dür W *Appl. Phys. B* **122** 50 (2016)
87. Borregaard J et al. *Phys. Rev. X* **10** 021071 (2020) https://doi.org/10.1103/PhysRevX.10.021071
88. Niu D et al. *npj Quantum Inf.* **9** 106 (2023)
89. Cabrillo C et al. *Phys. Rev. A* **59** 1025 (1999)
90. Feng X-L et al. *Phys. Rev. Lett.* **90** 217902 (2003)
91. Duan L-M, Kimble H J *Phys. Rev. Lett.* **90** 253601 (2003)
92. Simon C, Irvine W T M *Phys. Rev. Lett.* **91** 110405 (2003)
93. Barrett S D, Kok P *Phys. Rev. A* **71** 060310 (2005)
94. van Loock P et al. *Phys. Rev. A* **78** 062319 (2008)
95. Sangouard N, Dubessy R, Simon C *Phys. Rev. A* **79** 042340 (2009)
96. Krastanov S et al. *Phys. Rev. Lett.* **127** 040503 (2021)
97. Duan L-M et al. *Nature* **414** 413 (2001)
98. Simon C et al. *Phys. Rev. Lett.* **98** 190503 (2007)
99. Sangouard N et al. *Phys. Rev. A* **76** 050301 (2007)
100. Zhao B et al. *Phys. Rev. Lett.* **98** 240502 (2007)
101. Sangouard N et al. *Phys. Rev. A* **77** 062301 (2008)
102. Han Y et al. *Phys. Rev. A* **81** 052311 (2010)
103. Zhao B et al. *Phys. Rev. A* **81** 052329 (2010)
104. Minář J, de Riedmatten H, Sangouard N *Phys. Rev. A* **85** 032313 (2012)
105. Li C-L, Yin H-L, Chen Z-B *Rep. Prog. Phys.* **87** 127901 (2024)
106. Jones C et al. *New J. Phys.* **18** 083015 (2016)
107. van Loock P et al. *Adv. Quantum Technol.* **3** 1900141 (2020)
108. Daiss S et al. *Science* **371** 614 (2021)
109. Welte S et al. *Nat. Photon.* **15** 504 (2021)
110. Langenfeld S et al. *Phys. Rev. Lett.* **126** 130502 (2021)
111. Duan L-M, Kimble H J *Phys. Rev. Lett.* **92** 127902 (2004)
112. Reiserer A et al. *Nature* **508** 237 (2014)
113. Brekenfeld M et al. *Nat. Phys.* **16** 647 (2020)
114. Cirac J I et al. *Phys. Rev. Lett.* **78** 3221 (1997)
115. Ritter S et al. *Nature* **484** 195 (2012)
116. Ainley E M et al., arXiv:2408.00149
117. Childress L et al. *Phys. Rev. Lett.* **96** 070504 (2006)
118. Jiang L, Taylor J M, Lukin M D *Phys. Rev. A* **76** 012301 (2007)
119. Chen Z-B et al. *Phys. Rev. A* **76** 022329 (2007)
120. Yin Z-Q et al. *Phys. Rev. A* **79** 044302 (2009)
121. Wang T-J et al. *Phys. Rev. A* **85** 062311 (2012)
122. Li T, Yang G-J, Deng F-G *Phys. Rev. A* **93** 012302 (2016)
123. Jiang L et al. *Phys. Rev. A* **79** 032325 (2009)
124. Munro W J et al. *Nat. Photon.* **4** 792 (2010)
125. Fowler A G et al. *Phys. Rev. Lett.* **104** 180503 (2010)
126. Jing Y, Alsina D, Razavi M *Phys. Rev. Appl.* **14** 064037 (2020)
127. Jing Y, Razavi M *Phys. Rev. Appl.* **15** 044027 (2021)
128. Munro W J et al. *Nat. Photon.* **6** 777 (2012)
129. Muralidharan S et al. *Phys. Rev. Lett.* **112** 250501 (2014)
130. Bratzik S, Kampermann H, Bruß D *Phys. Rev. A* **89** 032335 (2014)
131. Namiki R et al. *Phys. Rev. A* **94** 052304 (2016)
132. Muralidharan S et al. *Phys. Rev. A* **97** 052316 (2018)
133. Glaudell A N, Waks E, Taylor J M *New J. Phys.* **18** 093008 (2016)
134. Ewert F, Bergmann M, van Loock P *Phys. Rev. Lett.* **117** 210501 (2016)
135. Ewert F, van Loock P *Phys. Rev. A* **95** 012327 (2017)
136. Zhan Y et al. *Quantum* **7** 924 (2023)
137. Wo K J et al. *npj Quantum Inf.* **9** 123 (2023)
138. Schmidt F, Miller D, van Loock P *Phys. Rev. A* **109** 042427 (2024)
139. Pettersson L, Sørensen A S, arXiv:2503.19822
140. Li Z-D et al. *Nat. Photon.* **13** 644 (2019)
141. Bennett C H, DiVincenzo D P, Smolin J A *Phys. Rev. Lett.* **78** 3217 (1997)
142. Muralidharan S et al. *Sci. Rep.* **6** 20463 (2016)
143. Collins O A et al. *Phys. Rev. Lett.* **98** 060502 (2007)
144. Azuma K et al. *AVS Quantum Sci.* **3** 014101 (2021)
145. Bernardes N K, Praxmeyer L, van Loock P *Phys. Rev. A* **83** 012323 (2011)

146. Shchukin E, Schmidt F, van Loock P *Phys. Rev. A* **100** 032322 (2019)
147. Coopmans T, Brand S, Elkouss D *Phys. Rev. A* **105** 012608 (2022)
148. Xie Y-M et al. *PRX Quantum* **3** 020315 (2022)
149. Zeng P et al. *Nat. Commun.* **13** 3903 (2022)
150. Wu Y, Liu J, Simon C *Phys. Rev. A* **101** 042301 (2020)
151. Shchukin E, van Loock P *Phys. Rev. Lett.* **128** 150502 (2022)
152. Avis G, Krastanov S *Phys. Rev. Research* **7** 033111 (2025); arXiv:2501.06291
153. Kamin L et al. *Phys. Rev. Research* **5** 023086 (2023)
154. Laurenza R et al. *Phys. Rev. Research* **4** 023158 (2022)
155. Jiang L et al. *Proc. Natl. Acad. Sci. USA* **104** 17291 (2007)
156. Wallnöfer J et al. *PRX Quantum* **5** 010351 (2024)
157. Razavi M, Piani M, Lütkenhaus N *Phys. Rev. A* **80** 032301 (2009)
158. Simon C, de Riedmatten H, Afzelius M *Phys. Rev. A* **82** 010304 (2010)
159. Sinclair N et al. *Phys. Rev. Lett.* **113** 053603 (2014)
160. van Dam S B et al. *Quantum Sci. Technol.* **2** 034002 (2017)
161. Liu X et al. *Phys. Rev. A* **95** 012319 (2017)
162. Huie W et al. *Phys. Rev. Research* **3** 043154 (2021)
163. Dhara P et al. *Phys. Rev. A* **105** 022623 (2022)
164. Zheng Y, Sharma H, Borregaard J *PRX Quantum* **3** 040319 (2022)
165. Childress L et al. *Phys. Rev. A* **72** 052330 (2005)
166. Asadi F K et al. *Quantum* **2** 93 (2018)
167. Simon C et al. *Eur. Phys. J. D* **58** 1 (2010)
168. Hammerer K, Sørensen A S, Polzik E S *Rev. Mod. Phys.* **82** 1041 (2010)
169. Tittel W et al. *Laser Photon. Rev.* **4** 244 (2010)
170. Bussières F et al. *J. Mod. Opt.* **60** 1519 (2013)
171. Heshami K et al. *J. Mod. Opt.* **63** 2005 (2016)
172. Chanelière T, Hétet G, Sangouard N *Adv. Atom. Mol. Opt. Phys.* **67** 77 (2018)
173. Hua Y-L et al. *Chinese Phys. B* **27** 020303 (2018)
174. Guo M et al. *Front. Phys.* **18** 21303 (2023)
175. Lei Y et al. *Optica* **10** 1511 (2023)
176. Moiseev S A et al. *Phys. Usp.* **68** 431 (2025); *Usp. Fiz. Nauk* **195** 455 (2025)
177. Fleischhauer M, Imamoglu A, Marangos J P *Rev. Mod. Phys.* **77** 633 (2005)
178. Finkelstein R et al. *New J. Phys.* **25** 035001 (2023)
179. Fleischhauer M, Lukin M D *Phys. Rev. Lett.* **84** 5094 (2000)
180. Lukin M D, Yelin S F, Fleischhauer M *Phys. Rev. Lett.* **84** 4232 (2000)
181. Manz S et al. *Phys. Rev. A* **75** 040101 (2007)
182. Novikova I, Walsworth R L, Xiao Y *Laser Photon. Rev.* **6** 333 (2012)
183. Liu C et al. *Nature* **409** 490 (2001)
184. Longdell J J et al. *Phys. Rev. Lett.* **95** 063601 (2005)
185. Hsiao Y-F et al. *Phys. Rev. Lett.* **120** 183602 (2018)
186. Nunn J et al. *Phys. Rev. A* **75** 011401 (2007)
187. Nunn J et al. *Phys. Rev. A* **96** 012338 (2017)
188. Hétet G et al. *Opt. Lett.* **33** 2323 (2008)
189. Zhang X, Kalachev A, Kocharovskaya O *Phys. Rev. A* **87** 013811 (2013)
190. Kalachev A, Kocharovskaya O *Phys. Rev. A* **88** 033846 (2013)
191. Alexander A L et al. *Phys. Rev. Lett.* **96** 043602 (2006)
192. Lauritzen B et al. *Phys. Rev. Lett.* **104** 080502 (2010)
193. Hétet G et al. *Phys. Rev. Lett.* **100** 023601 (2008)
194. Hedges M P et al. *Nature* **465** 1052 (2010)
195. Hosseini M et al. *Nat. Commun.* **2** 174 (2011)
196. Nunn J et al. *Phys. Rev. Lett.* **101** 260502 (2008)
197. Moiseev S A, Andrianov S N, Gubaidullin F F *Phys. Rev. A* **82** 022311 (2010)
198. Afzelius M, Simon C *Phys. Rev. A* **82** 022310 (2010)
199. de Riedmatten H et al. *Nature* **456** 773 (2008)
200. Afzelius M et al. *Phys. Rev. A* **79** 052329 (2009)
201. Lauritzen B et al. *Phys. Rev. A* **83** 012318 (2011)
202. Liu C et al. *Phys. Rev. Lett.* **125** 260504 (2020)
203. Craiciu I et al. *Optica* **8** 114 (2021)
204. Horvath S P et al. *Phys. Rev. Research* **3** 023099 (2021)
205. Duranti S et al. *Opt. Express* **32** 26884 (2024)
206. Akhmedzhanov R A et al. *Laser Phys. Lett.* **13** 115203 (2016)
207. Moiseev S A et al. *Phys. Rev. Lett.* **134** 070803 (2025)
208. Damon V et al. *New J. Phys.* **13** 093031 (2011)
209. Dajczgewand J et al. *New J. Phys.* **17** 023031 (2015)
210. Lan S-Y et al. *Opt. Express* **17** 13639 (2009)
211. Pu Y-F et al. *Nat. Commun.* **8** 15359 (2017)
212. Wang S et al. *Commun. Phys.* **4** 168 (2021)
213. Zhang S et al. *Nat. Commun.* **15** 10306 (2024)
214. Wang M et al. *Optica* **12** 274 (2025)
215. Sekatski P et al. *Phys. Rev. A* **83** 053840 (2011)
216. Kutluer K, Mazzera M, de Riedmatten H *Phys. Rev. Lett.* **118** 210502 (2017)
217. Laplane C et al. *Phys. Rev. Lett.* **118** 210501 (2017)
218. Krutyanskiy V et al. *PRX Quantum* **5** 020308 (2024)
219. You B et al., arXiv:2405.10501
220. Ruskuc A et al. *Nature* **639** 54 (2025)
221. Cui Z-B et al., arXiv:2503.13898
222. Kuhn A, Ljunggren D *Contemp. Phys.* **51** 289 (2010)
223. Reiserer A, Rempe G *Rev. Mod. Phys.* **87** 1379 (2015)
224. Reiserer A *Rev. Mod. Phys.* **94** 041003 (2022)
225. Covey J P, Weinfurter H, Bernien H *npj Quantum Inf.* **9** 90 (2023)
226. Kuhn A et al. *Appl. Phys. B* **69** 373 (1999)
227. Moehring D L et al. *Nature* **449** 68 (2007)
228. Hofmann J et al. *Science* **337** 72 (2012)
229. Boozer A D et al. *Phys. Rev. Lett.* **98** 193601 (2007)
230. Specht H P et al. *Nature* **473** 190 (2011)
231. Thiel C W, Böttger T, Cone R L *J. Luminescence* **131** 353 (2011)
232. Thiel C et al. *J. Phys. B* **45** 124013 (2012)
233. Popova M N *Opt. Spectrosc.* **119** 544 (2015); *Opt. Spektrosk.* **119** 541 (2015)
234. Yang W, Wang Z-Y, Liu R-B *Front. Phys. China* **6** 2 (2011)
235. Suter D, Álvarez G A *Rev. Mod. Phys.* **88** 041001 (2016)
236. Fraval E, Sellars M J, Longdell J J *Phys. Rev. Lett.* **92** 077601 (2004)
237. Longdell J J, Alexander A L, Sellars M J *Phys. Rev. B* **74** 195101 (2006)
238. Zhong M et al. *Nature* **517** 177 (2015)
239. Wang F et al. *PRX Quantum* **6** 010302 (2025)
240. Könz F et al. *Phys. Rev. B* **68** 085109 (2003)
241. Kukharchyk N et al. *New J. Phys.* **20** 023044 (2018)
242. Craiciu I et al. *Phys. Rev. Appl.* **12** 024062 (2019)
243. Li P-Y et al. *J. Luminescence* **225** 117344 (2020)
244. Fukumori R et al. *Phys. Rev. B* **101** 214202 (2020)
245. Gupta S et al. *Phys. Rev. Applied* **19** 044029 (2023)
246. Gangloff D A et al. *Science* **364** 62 (2019)
247. Appel M H et al. *Nat. Phys.* **21** 368 (2025)
248. Dyte H E et al., arXiv:2502.11092
249. Katz O, Firstenberg O *Nat. Commun.* **9** 2074 (2018)
250. Katz O, Shaham R, Firstenberg O *Sci. Adv.* **7** eabe9164 (2021)
251. Ji J-W et al. *Phys. Rev. Applied* **19** 054063 (2023)
252. Barbosa A, Terças H, Cruzeiro E Z, arXiv:2402.17752
253. Wang Y et al., arXiv:2503.11564
254. Li H et al. *Optica* **8** 925 (2021)
255. Dudin Y O, Li L, Kuzmich A *Phys. Rev. A* **87** 031801 (2013)
256. Tian Z et al. *Optica* **11** 1391 (2024)
257. Heinze G, Hubrich C, Halfmann T *Phys. Rev. Lett.* **111** 033601 (2013)
258. Ma Y et al. *Nat. Commun.* **12** 2381 (2021)
259. Yang S-J et al. *Nat. Photon.* **10** 381 (2016)
260. Stas P-J et al. *Science* **378** 557 (2022)
261. Grimm N et al. *Phys. Rev. Lett.* **134** 043603 (2025)
262. Tan T R et al. *Nature* **528** 380 (2015)
263. Inlek I V et al. *Phys. Rev. Lett.* **118** 250502 (2017)
264. Wang P et al. *Nat. Commun.* **12** 233 (2021)
265. Santra S et al. *New J. Phys.* **21** 073002 (2019)
266. Gu F et al., arXiv:2401.12395
267. Cussenot P et al., arXiv:2501.18704
268. Wang Y et al. *Nat. Photon.* **13** 346 (2019)
269. Cao M et al. *Optica* **7** 1440 (2020)
270. Sabooni M et al. *Phys. Rev. Lett.* **110** 133604 (2013)
271. Sparkes B M et al. *New J. Phys.* **15** 085027 (2013)
272. Jobez P et al. *New J. Phys.* **16** 083005 (2014)
273. Cho Y-W et al. *Optica* **3** 100 (2016)
274. Leung A C et al. *APL Quantum* **1** 036102 (2024)
275. Guo J et al. *Nat. Commun.* **10** 148 (2019)
276. England D G et al. *Phys. Rev. Lett.* **114** 053602 (2015)
277. Reim K F et al. *Phys. Rev. Lett.* **107** 053603 (2011)

278. England D G et al. *J. Phys. B* **45** 124008 (2012)
279. Usmani I et al. *Nat. Commun.* **1** 12 (2010)
280. Bonarota M, Le Gouët J-L, Chanelière T *New J. Phys.* **13** 013013 (2011)
281. Businger M et al. *Nat. Commun.* **13** 6438 (2022)
282. Xu Z et al. *Phys. Rev. Lett.* **111** 240503 (2013)
283. Zugenmaier M et al. *Commun. Phys.* **1** 76 (2018)
284. Dideriksen K B et al. *Nat. Commun.* **12** 3699 (2021)
285. Gómez-López E et al., arXiv:2503.22423
286. Holzäpfel A et al. *New J. Phys.* **22** 063009 (2020)
287. Kutluer K et al. *Phys. Rev. A* **93** 040302 (2016)
288. Hain M, Stabel M, Halfmann T *New J. Phys.* **24** 023012 (2022)
289. Ma L et al. *Nat. Commun.* **13** 2368 (2022)
290. Zhou Z-Q et al. *Phys. Rev. Lett.* **108** 190505 (2012)
291. Akhmedzhanov R A et al. *Laser Phys. Lett.* **20** 015204 (2023)
292. Akhmedzhanov R A et al. *Radiophys. Quantum Electron.* **67** 106 (2024); *Izv. Vyssh. Uchebn. Zaved. Radiofiz.* **67** 121 (2024)
293. Zhu T-X et al. *Phys. Rev. Lett.* **128** 180501 (2022)
294. Alqedra M K et al. *Phys. Rev. A* **109** 012607 (2024)
295. Zhou Z-Q et al. *Laser Photon. Rev.* **17** 2300257 (2023)
296. Liu D-C et al. *Phys. Rev. Lett.* **129** 210501 (2022)
297. Zhu T-X et al. *Natl. Sci. Rev.* **11** nwae161 (2024)
298. Liu U-P et al. *Sci. Adv.* **11** eadu5264 (2025)
299. Askarani M F et al. *Phys. Rev. Applied* **11** 054056 (2019)
300. Ma Y-Z et al. *Nat. Commun.* **12** 4378 (2021)
301. Wan N H et al. *Nature* **583** 226 (2020)
302. Keil M et al. *J. Mod. Opt.* **63** 1840 (2016)
303. Lago-Rivera D et al. *Nat. Commun.* **14** 1889 (2023)
304. Saglamyurek E et al. *Nat. Commun.* **7** 11202 (2016)
305. Chakraborty T et al. *npj Quantum Inf.* **11** 3 (2025)
306. Parniak M et al. *Nat. Commun.* **8** 2140 (2017)
307. Chang W et al. *Phys. Rev. X* **9** 041033 (2019) https://doi.org/10.1103/PhysRevX.9.041033
308. Cox K C et al. *Phys. Rev. Lett.* **123** 263601 (2019)
309. Yang T-S et al. *Nat. Commun.* **9** 3407 (2018)
310. Seri A et al. *Phys. Rev. Lett.* **123** 080502 (2019)
311. Li C et al. *PRX Quantum.* **2** 040307 (2021)
312. Wei S-H et al. *npj Quantum Inf.* **10** 19 (2024)
313. Shi B-S, Ding D-S, Zhang W *J. Phys. B* **51** 032004 (2018)
314. Nicolas A et al. *Nat. Photon.* **8** 234 (2014)
315. Ding D-S et al. *Phys. Rev. A* **90** 042301 (2014)
316. Ye Y-H et al. *Phys. Rev. Lett.* **129** 193601 (2022)
317. Yang X et al., arXiv:2503.01106
318. Dajczgewand J et al. *Opt. Lett.* **39** 2711 (2014)
319. Rančić M et al. *Nat. Phys.* **14** 50 (2018)
320. Ortu A et al. *npj Quantum Inf.* **8** 29 (2022)
321. Kako S et al. *Nat. Mater.* **5** 887 (2006)
322. Strauf S et al. *Nat. Photon.* **1** 704 (2007)
323. Shields A J *Nat. Photon.* **1** 215 (2007)
324. Senellart P, Solomon G, White A *Nat. Nanotechnol.* **12** 1026 (2017)
325. Arakawa Y, Holmes M J *Appl. Phys. Rev.* **7** 021309 (2020)
326. Zajac J M, Huber-Loyola T, Hofling S, arXiv:2503.13775
327. Chu X-L, Götzinger S, Sandoghdar V *Nat. Photon.* **11** 58 (2017)
328. De Martini F, Di Giuseppe G, Marrocco M *Phys. Rev. Lett.* **76** 900 (1996)
329. Kuhn A, Hennrich M, Rempe G *Phys. Rev. Lett.* **89** 067901 (2002)
330. Blinov B B et al. *Nature* **428** 153 (2004)
331. Maurer C et al. *New J. Phys.* **6** 94 (2004)
332. Kurtsiefer C et al. *Phys. Rev. Lett.* **85** 290 (2000)
333. Alléaume R et al. *New J. Phys.* **6** 92 (2004)
334. Babinec T M et al. *Nat. Nanotechnol.* **5** 195 (2010)
335. Dudin Y O, Kuzmich A *Science* **336** 887 (2012)
336. Castelletto S A, Scholten R E *Eur. Phys. J. Appl. Phys.* **41** 181 (2008)
337. Eisaman M D et al. *Rev. Sci. Instrum.* **82** 071101 (2011)
338. Caspani L et al. *Light Sci. Appl.* **6** e17100 (2017)
339. Signorini S, Pavesi L *AVS Quantum Sci.* **2** 041701 (2020)
340. Imamoğlu A et al. *Phys. Rev. Lett.* **79** 1467 (1997)
341. Birnbaum K M et al. *Nature* **436** 87 (2005)
342. Meyer-Scott E, Silberhorn C, Migdall A *Rev. Sci. Instrum.* **91** 041101 (2020)
343. Zhang C et al. *Adv. Quantum Technol.* **4** 2000132 (2021)
344. Adam P, Mechler M *Appl. Sci.* **14** 11249 (2024)
345. Ding X et al. *Nat. Photon.* **19** 387 (2025)
346. Varnava M, Browne D E, Rudolph T *Phys. Rev. Lett.* **100** 060502 (2008)
347. Tomm N et al. *Nat. Nanotechnol.* **16** 399 (2021)
348. Kim J-H et al. *Optica* **3** 577 (2016)
349. Kolatschek S et al. *Nano Lett.* **21** 7740 (2021)
350. Yu Y et al. *Nat. Nanotechnol.* **18** 1389 (2023)
351. Sempere-Llagostera S et al. *Opt. Express* **30** 3138 (2022)
352. Davis S I et al. *Phys. Rev. Appl.* **18** 064007 (2022)
353. Stasi L et al. *Quantum Sci. Technol.* **8** 045006 (2023)
354. Christ A, Silberhorn C *Phys. Rev. A* **85** 023829 (2012)
355. Ding C et al., arXiv:2504.02202
356. Cheng R et al. *Nat. Photon.* **17** 112 (2023)
357. Lu C-Y, Pan J-W *Nat. Photon.* **8** 174 (2014)
358. Anwar A et al. *Rev. Sci. Instrum.* **92** 041101 (2021)
359. Weiss T F, Peruzzo A *Appl. Phys. Rev.* **12** 011318 (2025)
360. Zhong H-S et al. *Phys. Rev. Lett.* **121** 250505 (2018)
361. Slattery O et al. *J. Res. Natl. Inst. Stand. Technol.* **124** 124019 (2019)
362. Ma Z et al. *Phys. Rev. Lett.* **125** 263602 (2020)
363. Rambach M et al. *APL Photonics* **1** 096101 (2016)
364. Rambach M et al. *Phys. Rev. Lett.* **121** 093603 (2018)
365. Liu J et al. *APL Photonics* **5** 066105 (2020)
366. He H et al. *Front. Phys.* **18** 61303 (2023)
367. Scholz M et al. *Appl. Phys. Lett.* **94** 201105 (2009)
368. Monteiro F et al. *Opt. Express* **22** 4371 (2014)
369. Slattery O et al. *Appl. Phys. B* **121** 413 (2015)
370. Tsai P-J, Chen Y-C *Quantum Sci. Technol.* **3** 034005 (2018)
371. Latypov I Z et al. *Quantum Electron.* **47** 827 (2017); *Kvantovaya Elektron.* **47** 827 (2017)
372. Luo K-H et al. *Opt. Express* **28** 3215 (2020)
373. Liu Y-C et al. *Sci. Rep.* **11** 12628 (2021)
374. Liu Y-C et al. *Photon. Res.* **9** 1998 (2021)
375. Kuo P S et al. *Opt. Quantum* **1** 43 (2023)
376. Gao M-Y et al. *Phys. Rev. Applied* **21** 034029 (2024)
377. Pomarico E et al. *New J. Phys.* **14** 033008 (2012)
378. Gao M-Y et al. *Phys. Rev. A* **109** 033720 (2024)
379. Seri A et al. *Phys. Rev. X* **7** 021028 (2017)
380. Seri A et al. *Optica* **5** 934 (2018)
381. Rakonjac J V et al. *Opt. Quantum* **1** 94 (2023)
382. Turaykhanov D A et al. *Radiophys. Quantum Electron.* **67** 80 (2024); *Izv. Vyssh. Uchebn. Zaved. Radiofiz.* **67** (1) 91 (2024)
383. Chang K-C et al. *Newton* **1** 100024 (2025)
384. Xie Z et al. *Nat. Photon.* **9** 536 (2015)
385. Chang K-C et al. *npj Quantum Inf.* **7** 48 (2021)
386. Yamazaki T et al. *Sci. Rep.* **12** 8964 (2022)
387. Cheng X et al. *Commun. Phys.* **6** 278 (2023)
388. Wen W et al. *Phys. Rev. Applied* **20** 064032 (2023)
389. Reimer C et al. *Nat. Phys.* **15** 148 (2019)
390. Roh C et al. *Nat. Photon.* **19** 526 (2025)
391. Ikuta R et al. *Phys. Rev. Lett.* **123** 193603 (2019)
392. Krovi H et al. *Appl. Phys. B* **122** 52 (2016)
393. Lu H-H et al. *Optica* **10** 1655 (2023)
394. Lee D et al. *Light Sci. Appl.* **13** 90 (2024)
395. Mueller A et al. *Opt. Quantum* **2** 64 (2024)
396. Chuprina I N, Kalachev A A *Phys. Rev. A* **100** 043843 (2019)
397. Young R J et al. *New J. Phys.* **8** 29 (2006)
398. Akopian N et al. *Phys. Rev. Lett.* **96** 130501 (2006)
399. Schimpf C et al. *Appl. Phys. Lett.* **118** 100502 (2021)
400. Wang H et al. *Phys. Rev. Lett.* **122** 113602 (2019)
401. Rota M B et al. *eLight* **4** 13 (2024)
402. Liu J et al. *Nat. Nanotechnol.* **14** 586 (2019)
403. Kumar P *Opt. Lett.* **15** 1476 (1990)
404. Lauk N et al. *Quantum Sci. Technol.* **5** 020501 (2020)
405. Han X et al. *Optica* **8** 1050 (2021)
406. O'Sullivan J et al. *Nat. Commun.* **16** 5505 (2025); arXiv:2409.06623
407. Higginbotham A P et al. *Nat. Phys.* **14** 1038 (2018)
408. Xu X et al. *Micromachines* **15** 485 (2024)
409. Pelc J S et al. *Opt. Express* **19** 21445 (2011)
410. Ma L, Slattery O, Tang X *Phys. Rep.* **521** 69 (2012)
411. Liao S-K et al. *Nat. Photon.* **11** 509 (2017)
412. Albrecht B et al. *Nat. Commun.* **5** 3376 (2014)
413. Ikuta R et al. *Nat. Commun.* **9** 1997 (2018)
414. Bock M et al. *Nat. Commun.* **9** 1998 (2018)
415. Yu Y et al. *Nature* **578** 240 (2020)

416. van Leent T et al. *Phys. Rev. Lett.* **124** 010510 (2020)
417. Luo X-Y et al. *Phys. Rev. Lett.* **129** 050503 (2022)
418. van Leent T et al. *Nature* **607** 69 (2022)
419. Krutyanskiy V et al. *Phys. Rev. Lett.* **130** 213601 (2023)
420. Bersin E et al. *PRX Quantum* **5** 010303 (2024)
421. Takesue H *Phys. Rev. Lett.* **101** 173901 (2008)
422. Qu L-Y et al. *Phys. Rev. Lett.* **123** 243601 (2019)
423. Han Z-Q-Z et al. *Adv. Devices Instrum.* **4** 0030 (2023)
424. Zeuthen E et al. *Quantum Sci. Technol.* **5** 034009 (2020)
425. Wang C-H, Li F, Jiang L *Nat. Commun.* **13** 6698 (2022)
426. Maring N et al. *Optica* **5** 507 (2018)
427. Fernandez-Gonzalvo X et al. *Opt. Express* **21** 19473 (2013)
428. Samblowski A et al. *Opt. Lett.* **39** 2979 (2014)
429. Mann F et al. *Phys. Rev. Applied* **20** 054010 (2023)
430. Li Q, Davanço M, Srinivasan K *Nat. Photon.* **10** 406 (2016)
431. Guo X et al. *Phys. Rev. Lett.* **117** 123902 (2016)
432. Radnaev A G et al. *Nat. Phys.* **6** 894 (2010)
433. Bustard P J et al. *Phys. Rev. A* **95** 053816 (2017)
434. Zhou Z Y et al. *Light Sci. Appl.* **5** e16019 (2016)
435. De Greve K et al. *Nature* **491** 421 (2012)
436. Lio B D et al. *Adv. Quantum Technol.* **5** 2200006 (2022)
437. Zaske S et al. *Phys. Rev. Lett.* **109** 147404 (2012)
438. Esfandyarpour V, Langrock C, Fejer M *Opt. Lett.* **43** 5655 (2018)
439. Pelc S et al. *Opt. Lett.* **35** 2804 (2010)
440. Lu X et al. *Opt. Lett.* **46** 222 (2021)
441. Wright L J et al. *Phys. Rev. Lett.* **118** 023601 (2017)
442. Grimau Puigibert M et al. *Phys. Rev. Lett.* **119** 083601 (2017)
443. Hiemstra T et al. *Phys. Rev. Applied* **14** 014052 (2020)
444. Yu H et al. *Photon. Res.* **10** 1417 (2022)
445. Joshi C et al. *Nat. Commun.* **9** 847 (2018)
446. Wang P-C et al. *J. Opt. Soc. Am. B* **38** 1140 (2021)
447. Rosenfeld W et al. *Phys. Rev. Lett.* **119** 010402 (2017)
448. Hucul D et al. *Nat. Phys.* **11** 37 (2015)
449. Stephenson L J et al. *Phys. Rev. Lett.* **124** 110501 (2020)
450. Krutyanskiy V et al. *Phys. Rev. Lett.* **130** 050803 (2023)
451. Saha S et al. *Nat. Commun.* **16** 2533 (2025)
452. Bernien H et al. *Nature* **497** 86 (2013)
453. Hensen B et al. *Nature* **526** 682 (2015)
454. Humphreys P C et al. *Nature* **558** 268 (2018)
455. Stolk A J et al. *Sci. Adv.* **10** eadp6442 (2024)
456. Delteil A et al. *Nat. Phys.* **12** 218 (2016)
457. Stockill R et al. *Phys. Rev. Lett.* **119** 010503 (2017)
458. Chou C W et al. *Nature* **438** 828 (2005)
459. Yuan Z-S et al. *Nature* **454** 1098 (2008)
460. Pu Y-F et al. *Nat. Photon.* **15** 374 (2021)
461. Chou C-W et al. *Science* **316** 1316 (2007)
462. Lago-Rivera D et al. *Nature* **594** 37 (2021)
463. Liu X et al. *Nature* **594** 41 (2021)
464. Nguyen C T et al. *Phys. Rev. Lett.* **123** 183602 (2019)
465. Zhang W et al. *Nature* **607** 687 (2022)
466. Nadlinger D P et al. *Nature* **607** 682 (2022)
467. Yin J et al. *Science* **356** 1140 (2017)
468. Bhaskar M K et al. *Nature* **580** 60 (2020)
469. Lo H-K, Curty M, Qi B *Phys. Rev. Lett.* **108** 130503 (2012)
470. Langenfeld S et al. *Phys. Rev. Lett.* **126** 230506 (2021)
471. Pompili M et al. *Science* **372** 259 (2021)
472. Hermans S L N et al. *Nature* **605** 663 (2022)
473. Bonato C et al. *New J. Phys.* **11** 045017 (2009)
474. Bourgoin J-P et al. *New J. Phys.* **15** 023006 (2013)
475. Hosseinidehaj N et al. *IEEE Commun. Surv. Tutorials* **21** 881 (2018)
476. Dequal D et al. *npj Quantum Inf.* **7** 3 (2021)
477. Brito S et al. *PRX Quantum* **2** 010304 (2021)
478. Vallone G et al. *Phys. Rev. Lett.* **115** 040502 (2015)
479. Takenaka H et al. *Nat. Photon.* **11** 502 (2017)
480. Liao S-K et al. *Phys. Rev. Lett.* **120** 030501 (2018)
481. Liao S-K et al. *Nature* **549** 43 (2017)
482. Ren J-G et al. *Nature* **549** 70 (2017)
483. Li Y et al. *Nature* **640** 47 (2025)
484. Vasylyev D, Vogel W, Moll F *Phys. Rev. A* **99** 053830 (2019)
485. Liorni C, Kampermann H, Bruß D *New J. Phys.* **21** 093055 (2019)
486. Liorni C, Kampermann H, Bruß D *New J. Phys.* **23** 053021 (2021)
487. Pirandola S *Phys. Rev. Research* **3** 023130 (2021)
488. Boone K et al. *Phys. Rev. A* **91** 052325 (2015)
489. Gündoğan M et al. *npj Quantum Inf.* **7** 128 (2021)
490. Wallnöfer J et al. *Commun. Phys.* **5** 169 (2022)
491. Gündoğan M et al. *Opt. Quantum* **2** 140 (2024)